Paired and solitary ionocytes in the zebrafish olfactory epithelium

Julia Peloggia[1,*], King Yee Cheung[2,3,*], Tanya T. Whitfield[3,^], Mariela D. Petkova[4], Richard Schalek[4], Jonathan Boulanger-Weill[4,5], Yuelong Wu[4], Shuohong Wang[4], Nicholas J. van Hateren[3], Michał Januszewski[6], Viren Jain[7], Jeff W. Lichtman[4], Florian Engert[4], Tatjana Piotrowski[1] and Suresh Jesuthasan[2,8,^].

*equal contribution

^corresponding authors: t.whitfield@sheffield.ac.uk, suresh.jesuthasan@umu.se

[1]Stowers Institute for Medical Research, Kansas City, MO 64110, USA.

[2]Lee Kong Chian School of Medicine, Nanyang Technological University, Singapore 636921.

[3]School of Biosciences, Bateson Centre and Neuroscience Institute, University of Sheffield, Sheffield, S10 2TN, United Kingdom.

[4]Department of Molecular and Cellular Biology, Center for Brain Science, Harvard University, Cambridge, MA 02138, USA.

[5]Sorbonne Université, Institut National de la Santé et de la Recherche Médicale, Centre National de la Recherche Scientifique, Institut de la Vision, Paris, France

[6]Google Research, Zürich 8002, Switzerland.

[7]Google Research, Mountain View, CA 94043, USA.

[8]Department of Molecular Biology, Umeå University, Sweden.

Short title: Gene expression and morphology of zebrafish olfactory ionocytes

Abstract

The sense of smell is generated by electrical currents that are influenced by the concentration of ions in olfactory sensory neurons and mucus. In contrast to the extensive morphological and molecular characterization of sensory neurons, there has been little description of the cells that control ion concentrations in the zebrafish olfactory system. Here, we report the molecular and ultrastructural characterization of zebrafish olfactory ionocytes. Transcriptome analysis suggests that the zebrafish olfactory epithelium contains at least three different ionocyte types, which resemble Na^+/K^+-ATPase-rich (NaR), Na^+/Cl^- cotransporter (NCC), and H^+-ATPase-rich (HR) cells, responsible for calcium, chloride, and pH regulation, respectively, in the zebrafish skin. NaR-like and HR-like ionocytes are usually adjacent to one another, whereas NCC-like cells are usually solitary. The distinct subtypes are differentially distributed: NaR-like/HR-like cell pairs are found broadly within the olfactory epithelium, whereas NCC-like cells reside within the peripheral non-sensory multiciliated cell zone. Comparison of gene expression and serial-section electron microscopy analysis indicates that the NaR-like cells wrap around the HR-like cells and are connected to them by shallow tight junctions. The development of olfactory ionocyte subtypes is also differentially regulated, as pharmacological Notch inhibition leads to a loss of NaR-like and HR-like cells, but does not affect NCC-like ionocyte number. These results provide a molecular and anatomical characterization of olfactory ionocytes in a stenohaline freshwater teleost. The paired ionocytes suggest that both transcellular and paracellular transport regulate ion concentrations in the olfactory epithelium, while the solitary ionocytes may enable independent regulation of multiciliated cells.

49 # Introduction

50 Olfaction is mediated by a combination of ion currents – an influx of calcium
51 followed by an efflux of chloride – that is triggered by the binding of an odorant to its
52 receptor on olfactory sensory neurons (OSNs) [1,2]. The high concentration of
53 chloride in the dendritic knobs and cilia of mammalian OSNs is achieved by uptake
54 from the mucus by the NKCC1 (Slc12a2) co-transporter, which requires external
55 sodium [3]. Despite the relative robustness of transduction that is offered by the
56 chloride current [4], olfactory sensitivity is influenced by external ion concentrations
57 [5]. The zebrafish, a freshwater fish that can be found in the wild in water with a
58 moderate range of salinity [6], has provided fundamental insights into olfactory
59 processing [7,8]. The morphological and molecular features of OSNs of this animal
60 are well described [9–11]. However, it is unclear how ion composition in the
61 zebrafish olfactory epithelium is regulated.

62 Ionocytes are mitochondria-rich cells that can transport ions intracellularly
63 against their concentration gradient. In freshwater teleosts, ionocytes in the skin and
64 gills actively absorb ions from the external environment, compensating for passive
65 water gain (reviewed in [12,13]). In marine teleosts, ionocytes in the kidneys and gills
66 actively secrete excess ions absorbed from seawater. Recently, with the advent of
67 single cell sequencing technologies, ionocytes have been identified based on gene
68 expression in several tissues including the olfactory epithelium in humans and mice
69 [14,15], inner ear of mice [16] and the lateral line neuromasts in zebrafish [17]. In the
70 neuromasts, as in the gill and skin of fish, a subset of ionocytes were found in a
71 complex; the presence of shallow tight junctions in such complexes [18] is thought to
72 provide an alternative paracellular pathway for ion movement, for example by
73 coupling Na^+ secretion to Cl^- efflux via the CFTR (cystic fibrosis transmembrane

conductance regulator) channel in an adjacent ionocyte in the gill of *Fundulus* in seawater [19] .

The existence of ionocytes in the olfactory epithelium of fish was first suggested in 1972 based on light and electron microscopy of Baltic Sea trout [20]. The cells, termed “labyrinth cells”, were characterised by an abundance of mitochondria as well as smooth endoplasmic reticulum, and were proposed to be functionally equivalent to “chloride cells” in the gill. A transmission electron microscopy (TEM) and scanning electron microscopy (SEM) study in 2001 confirmed the presence of cells with a similar appearance in the olfactory epithelium of seven freshwater fish species, and noted their distinct morphology: an apical surface with microvilli-like projections and occasional invaginations of the cell membrane [21]. Labyrinth cells were also recently identified in the freshwater goby, where they were described as having a globular appearance in scanning electron micrographs [22]. However, little is known about the molecular characteristics of these putative ionocytes, and it is not known if they exist in isolation or as complexes.

In mammals and frogs, the winged helix/forkhead transcription factor Foxi1 is required for ionocyte specification, and thus provides a useful marker for ionocytes. In zebrafish, the Foxi1 orthologs *foxi3a* and *foxi3b* regulate ionocyte development, and loss of *foxi3a* leads to complete loss of ionocytes [23,24]. Based on their *foxi3a* expression, several classes of epidermal and gill ionocytes in the zebrafish were discovered, including: H^+-ATPase-rich (HR) ionocytes which secrete protons, take up sodium, and excrete ammonium ions; Na^+/-K^+-ATPase-rich (NaR) ionocytes which take up calcium ions; Na^+/Cl^- co-transporter-expressing (NCC) ionocytes which take up sodium and chloride ions; and K^+-secreting (KS) ionocytes which secrete potassium ions (reviewed in [12,13,25]). The different classes of ionocytes possess

99 distinct gene expression profiles [13,17]; distinguishing markers include *trpv6* (for
100 NaR [26]), *ceacam1* (for HR [27]), and *slc12a10.2* (for NCC [28,29]). Here, we use
101 transcriptomic data, in situ hybridization and serial-section electron microscopy
102 (ssEM) to characterise the different subtypes of ionocytes in the zebrafish olfactory
103 epithelium.

104 Results

105 Single-cell RNA sequencing reveals the presence of several 106 classes of olfactory ionocytes

107 To search for potential ionocytes in the zebrafish olfactory epithelium, we
108 used single-cell RNA sequencing (scRNA-seq) datasets generated from dissected
109 adult olfactory rosettes [30]. We identified both major types of olfactory sensory
110 neurons (OSNs; ciliated and microvillous, marked by *ompb* and *trpc2b*, respectively),
111 supporting cells, neuronal progenitors and immune cell clusters (Fig. 1A, S1A–C).
112 Additionally, we found a cluster containing the well-conserved pan-ionocyte markers,
113 *foxi3a* and *foxi3b* [23,24]. Differential gene expression among clusters shows the
114 expression of NaR ionocyte genes such as *trpv6*, *gcm2*, *fxyd11* (*si:dkey-33i11.4*) [31]
115 and *atp1a1a.3* [32], and HR ionocyte markers, such as *ceacam1* (Fig. 1B–F; cluster
116 18 in Table S1). The cluster contains a high level of mitochondrial genes (Fig. S1D),
117 consistent with the mitochondria-rich characteristic of ionocytes. We did not detect
118 genes characteristic of other zebrafish ionocyte subtypes, such as *slc12a10.2* [28].
119 Differential expression analysis also indicated the expression of genes mediating
120 Notch-Delta signalling (e.g. *lfng*, *notch1b*), similar to what has been described in

121 different ionocyte subtypes [17,33]. These results suggest the presence of olfactory
122 ionocytes in the adult zebrafish.

123 To determine if olfactory ionocytes are present at larval stages, we searched
124 for the expression of ionocyte marker genes in scRNA-seq datasets from larval
125 zebrafish [34,35]. In addition to the expression in previously defined ionocyte
126 clusters, we found that the same genes were co-expressed in a small group of cells
127 within the larval olfactory epithelium cluster (Fig. 1H,I). Interestingly, in a separate
128 dataset from larval epithelial cells [17], we detected *foxi3b*$^+$ cells in the olfactory
129 epithelium cluster that do not express genes that mark NaR and HR cells. Differential
130 gene expression of these *foxi3b*$^+$ cells against the remaining cells revealed a
131 different set of ionocyte markers, including *slc12a10.2*, characteristic of NCC
132 ionocytes (Fig. 1J–M; Table S2).

133 Transcriptomic data thus suggest the presence of three distinct subtypes of
134 ionocytes in the larval olfactory epithelium and adult zebrafish olfactory rosette.
135 These subtypes have transcriptional signatures of skin NaR, HR and NCC ionocytes.

136 Spatial expression analysis identifies paired and solitary olfactory 137 ionocytes

138 To validate the transcriptomic data, and to determine the localization and
139 number of olfactory ionocytes in larval fish, we performed whole-mount fluorescent in
140 situ hybridization with hybridization chain reaction (HCR RNA-FISH) [36]. We initially
141 examined the expression of *foxi3b*, expressed in all ionocyte subtypes detected in
142 the olfactory transcriptomes, and *trpv6* and *ceacam1* to label the NaR and HR
143 ionocyte populations, respectively. *foxi3b*$^+$ cells were found in all regions of the
144 olfactory pit at 5 days post-fertilization (dpf), but were enriched in the postero-lateral

145 region (see white arrowhead; Fig. 2A–A'). There was a mean of 21 *foxi3b*$^{+}$ cells per
146 olfactory pit (*N* of olfactory pits = 6).

147 A subset of the *foxi3b*$^{+}$ cells expressed the HR marker *ceacam1* (Fig. 2B).
148 Interestingly, we always detected one *ceacam1*$^{+}$ (HR-like) cell adjacent to a *trpv6*$^{+}$
149 (NaR-like) cell (Fig. 2A–A''',C–C''). These pairs of cells typically had nuclei situated
150 deep in the epithelium, and each had an extension reaching the epithelial surface
151 (see magenta and cyan arrowheads, Fig. 2C; Movie S1). Notch pathway genes are
152 expressed in olfactory ionocytes (Fig. 1B). To test whether Notch signalling is active
153 in these pairs, we used the Notch reporter *Tg(tp1bglobin:EGFP)*^{um14} in combination
154 with HCR RNA-FISH. Notch signalling is active in one of the two cells of the ionocyte
155 pairs in the olfactory epithelium, with the NaR-like ionocyte (*trpv6*$^{+}$) being the Notch-
156 positive cell of the pair (Fig. 2D–D'').

157 To test which other ion channel genes are expressed in these cells, we
158 performed additional stainings for HR markers. Indeed, the *trpv6*$^{-}$ cell of the pair
159 expresses the sodium/proton transporter *slc9a3.2* (Fig. 2E) and the anion transporter
160 *slc4a1b* (Fig. 2F). However, these cells do not express the ammonium transporter
161 *rhcgb* (Fig. S2), which has been detected in HR ionocytes in the skin [37].

162 Besides the presence of *trpv6*$^{+}$ and *ceacam1*$^{+}$ ionocyte pairs, we also
163 observed solitary *foxi3b*$^{+}$ cells that were not paired with *ceacam1*$^{+}$ cells (Fig. 2C).
164 These cells were positioned on the lateral borders of the olfactory pit and had a
165 rounded morphology (see yellow arrowhead, Fig. 2C; Movie S2). To test if these
166 *foxi3b*$^{+}$ cells correspond to the NCC-like cells present in the larval epithelial dataset,
167 we performed HCR RNA-FISH, combining a *foxi3b* probe with different markers
168 obtained from differential expression analysis of scRNA-seq data. We confirmed that

169 these solitary *foxi3b*$^{+}$ cells express the NCC ionocyte markers *slc12a10.2, chrd* and
170 *hepacam2* [14,17] (Fig. 2G–I).

171 We used HCR RNA-FISH to examine the distribution of ionocytes in adult
172 zebrafish olfactory rosettes. Ionocyte pairs were detected throughout the rosette
173 (Fig. 3A–B'''); *trpv6*$^{+}$ cells were adjacent to a strongly *ceacam1*$^{+}$ cell throughout the
174 epithelium, with both cell types having varying levels of *foxi3b* expression (Fig.
175 3B''',C''',D'''). In the peripheral non-sensory region, by contrast, we additionally
176 observed *foxi3b*$^{+}$ cells with no expression of *trpv6* or *ceacam1* (Fig. 3C–E'''). These
177 NCC-like ionocytes appeared rounded in all cases (Fig 3D,D''',E,E'''; Fig. S3),
178 whereas NaR-like/HR-like ionocytes had variable morphologies, appearing
179 elongated in the region close to the OSN zone, and rounded in the most peripheral
180 non-sensory regions (Fig. 3D–E''').

181 We conclude that the zebrafish olfactory epithelium contains three main types
182 of ionocytes, at both larval and adult stages. One type is an NCC-like ionocyte,
183 which is solitary and expresses the chloride channel *slc12a10.2*. The other two
184 types, which are present in pairs, consist of one *trpv6*$^{+}$*,* NaR-like ionocyte and one
185 *ceacam*$^{+}$*,* HR-like ionocyte.

186 **Time-course of olfactory ionocyte development**

187 To determine when olfactory ionocytes appear during embryonic development
188 and their dynamics, we performed a time course analysis of *foxi3b* and *trpv6*
189 expression from 1 to 5 dpf (Fig. 4). None of the ionocyte subtypes were observed in
190 embryos at 1 dpf. Most olfactory pits showed solitary *foxi3b*$^{+}$ ionocytes at 2 dpf, while
191 paired ionocytes were not as frequent (Fig. 4A,B). The numbers of all olfactory
192 ionocyte subtypes progressively increased over time (Fig. 4A–C).

193 Besides the presence of mature ionocytes, we also detected *foxi3a*$^{+}$ cells
194 adjacent to the olfactory epithelium (Fig. S4A). These cells did not express any of the
195 ion channel genes we examined by HCR RNA-FISH. Similar cells have been
196 observed in the lateral line neuromast [17]. In these organs, neuromast ionocyte
197 progenitors are *krt1-19e*$^{+}$ skin cells which turn off expression of the ionocyte
198 specification transcription factor genes *foxi3a* and *foxi3b* as they invade neuromasts,
199 where they differentiate. To test if *krt1-19e*$^{+}$ cells give rise to new ionocytes in the
200 olfactory epithelium during development, we performed time-lapse analyses of the
201 transgenic line *Tg(krtt1c19e:lyn-tdTomato)*^{sq16}. While we observed several new
202 ionocytes invading the lateral line neuromasts, we did not observe any *tdTomato*$^{+}$
203 cells migrate into the olfactory pit (Fig. S2B,C; Movie S3). Additionally, olfactory pits
204 did not contain any *tdTomato*$^{+}$ cells, suggesting that these cells do not give rise to
205 ionocytes in the olfactory epithelium (Fig. S2B,C''). We cannot distinguish, however,
206 whether olfactory ionocytes are derived from *krt1-19e*$^{-}$ basal cells or if the transgenic
207 line does not label the population of basal cells surrounding the olfactory epithelium.

208 Notch signalling differentially regulates olfactory ionocyte number

209 Ionocyte differentiation and survival is regulated by Notch signalling in
210 different tissues [17,24,33]. To test if Notch signalling also plays a role in ionocyte
211 development and maintenance in the olfactory epithelium, we treated 4 dpf larvae for
212 24h with the gamma-secretase inhibitor LY411575, which inhibits Notch signalling
213 (Fig. 5A). We observed a striking loss of NaR- and HR-like pairs, but no change to
214 NCC-like ionocyte number in the olfactory epithelium (Fig. 5B–E). The remaining
215 NaR- and HR-like pairs show altered cell morphology, and could be undergoing cell
216 death (Fig. 5E).

217 In neuromast (Nm) ionocytes, transcription of the Notch ligand gene *dld* is
218 upregulated during division of the ionocyte progenitor cell into the NaR- and HR-like
219 pair, resulting in two *dld*$^{+}$ cells [17]. To investigate whether olfactory NaR- and HR-
220 like pairs develop in a similar manner, we performed time-lapse analysis of the
221 transgenic *dld* reporter line *Tg(dld:hist2h2l-EGFP)*^{psi84Tg} from 3–5 dpf. We observed
222 pairs of EGFP+ cells appear at the edge of the pit, upregulate EGFP and
223 differentiate into ionocytes (Movies S4, S5). These data suggest that, similar to Nm
224 ionocytes, NaR- and HR-like ionocyte pairs in the olfactory epithelium do not
225 originate from the division of pre-existing ionocyte pairs, but come from a different
226 population of progenitor cells.

227 Ultrastructure of larval zebrafish olfactory ionocytes

228 To describe the ultrastructure and three-dimensional shape of olfactory
229 ionocytes, we examined a serial-section electron microscopy (ssEM) dataset of a 7
230 dpf wild-type zebrafish larva. Here, we found mitochondria-rich cells in the olfactory
231 epithelium with ultrastructural features typical of teleost ionocytes [20,21,38–41]. An
232 extensive tubular network gave the cytoplasm a lacy appearance, quite distinct from
233 that of OSNs or other olfactory cell types, making it possible to spot these relatively
234 rare cell types. Consistent with the HCR RNA-fish data, the cells had differing shape
235 and appearance in different regions of the olfactory epithelium.

236 We found several examples of ionocytes within the OSN zone of the olfactory
237 pit (Fig. 6). These slender cells spanned almost the full width of the epithelium (>20
238 µm in apicobasal length), with nuclei positioned just above basal cells near the basal
239 lamina. In line with the transcriptomics data, most examples consisted of a pair of
240 cells. One member of the pair, which we propose is the HR-like cell (see below),
241 terminated in an apical knob bearing ~50 short, irregular microvilli, intermediate in

242 diameter (0.2 μm) between the microvilli of microvillous OSNs (0.1 μm diameter) and
243 the cilia of ciliated OSNs and non-sensory multiciliated cells (MCCs; 0.25–0.3 μm
244 diameter) (Fig. 6A,C,E,E'). Apart from a cortical zone at the cell apex, the cytoplasm
245 was densely packed with mitochondria in close association with an extensive
246 intracellular tubular network (Fig. 6C,D).

247 The HR-like ionocytes within the OSN zone were closely associated with a
248 second cell along most of their apicobasal length (Fig. 6). This second cell wrapped
249 around the HR-like ionocyte at the cell apex with a thin layer of cytoplasm, forming a
250 crescent in transverse section (Fig. 6A–E'''). At their apices, the two cells were
251 connected with a continuous shallow (0.1–0.2 μm) tight junction (zonula occludens),
252 and to surrounding cells with deep (0.5–1 μm) tight junctions (Fig. 6F,G,L). In a gap
253 not covered by the wrapping cell, the ionocyte was sealed to an olfactory supporting
254 cell by a deep tight junction (Fig. 6F,G). The cytoplasm of the wrapping cell also had
255 some ionocyte-like characteristics (e.g. some tubules and pores). The ultrastructure
256 of both cells of the pair was clearly distinct from the supporting cells that surround
257 and insulate the OSNs, which are full of secretory granules (Fig. 6C).

258 To determine which member of the cell pair corresponded to which type of
259 ionocyte, we compared the morphology of the ssEM 3D reconstructions to that of live
260 cells imaged at 5 dpf with the *Tg(tp1bglobin:EGFP)* Notch reporter line, which marks
261 the NaR-like ionocytes (Fig. 6H–K). The morphology of the live NaR-like cells clearly
262 matched that of the wrapping cells seen in the ssEM dataset, with a thin curved layer
263 of cytoplasm near the cell apex, sometimes appearing as a doublet in lateral view
264 (Fig. 6H,H'), and forming a clear crescent in a top-down view (Fig. 6K). Taken
265 together, the ssEM and fluorescence imaging data strongly suggest that the ionocyte
266 cell pairs found in the ssEM dataset correspond to the HR-like and NaR-like ionocyte

267 pairs identified through transcriptomic profiling, with the NaR-like cell wrapping
268 around the apex of the HR-like cell.
269 We also found occasional examples of multicellular ionocyte complexes
270 consisting of three or four cells within the OSN zone of the larval olfactory epithelium
271 (Fig. 6L–S). In one example (Fig. 6L–P), one HR-like/NaR-like pair was associated
272 with a second possible NaR-like cell. In this example, the HR-like ionocyte was
273 closely associated with a ciliated OSN at its base. In another example (Fig. 6Q), the
274 cell complex appeared to consist of an HR-like/NaR-like pair with a second possible
275 HR-like cell. We also found a four-cell complex consisting of a pair of HR-like/NaR-
276 like pairs, separate at their apices, but closely associated beneath the surface of the
277 epithelium (Fig. 6R,S).
278 Olfactory ionocytes with a different morphology were present in the MCC zone
279 at the periphery of the olfactory pit (Fig. 7). Here, the rounded microvillous apical
280 knobs of individual ionocytes could be identified by scanning electron microscopy
281 (SEM) in *ift88*$^{-/-}$ mutant larvae at 4 dpf (Fig. 7A–C). These mutants lack cilia, which
282 would otherwise obscure these cells in the wild type. Ionocytes were visible in the
283 olfactory pits of two out of three individuals. In the ssEM dataset of a wild-type larva
284 at 7 dpf, mitochondria-rich cells containing a dense tubular network were present
285 within the non-sensory zone of MCCs (Fig. 7D–M). Some of these peripheral
286 ionocytes were cuboidal in shape, without the long narrow neck of the ionocytes in
287 the central OSN zone, where the olfactory epithelium is thicker (Fig. 7D–I). Other
288 ionocytes in the MCC zone were more columnar in shape (Fig. 7J). Peripheral
289 ionocytes formed deep tight junctions with surrounding non-sensory MCCs, skin
290 cells, and other ionocytes. Basally, they were positioned just above the basal cells of
291 the olfactory epithelium (Fig. 7F,J), occasionally extending thin end-feet to contact

292 the basal lamina directly (Fig. 7M). However, they did not appear to be paired with,
293 or wrapped by, any other cell along their entire apicobasal length, in contrast to the
294 ionocytes in the OSN zone. Some, but not all, peripheral ionocytes had a large apical
295 knob bearing ~100 irregular microvilli, with part protruding from the epithelium (Fig.
296 7D,F), and part sunken to form a crypt or pit (Fig. 7G), matching the morphology
297 revealed by SEM at 4 dpf (Fig. 7C). Based on their location in the MCC zone and
298 morphology, and in comparison to the scRNA-seq data, we identify the cuboidal
299 peripheral olfactory ionocytes as NCC-like cells.

300 Discussion

301 Through analysis of single-cell transcriptomic, gene expression and volume
302 electron microscopy data, we have identified at least three subtypes of ionocytes in
303 the larval and adult zebrafish olfactory epithelium (Fig. 8). All three express the pan-
304 ionocyte marker *foxi3b*, but can be distinguished by transcriptomic signatures and
305 morphology. NaR-like ionocytes, expressing *trpv6*, were paired with HR-like
306 ionocytes, expressing *ceacam1* and the transporter genes *slc9a3.2* and *slc4a1b*.
307 NaR-like/HR-like cell pairs were situated throughout the olfactory epithelium,
308 including within sensory regions, with cell nuclei deep in the epithelium and a long
309 protrusion extending to the epithelial surface. NCC-like ionocytes, expressing
310 *slc12a10.2*, *chrd*, and *hepacam2*, were located exclusively in the multiciliated cell
311 zone of the larval olfactory pit, posterolaterally distributed, and more rounded in
312 shape. Solitary ionocytes lacking *trpv6* and *ceacam1* were also seen in the non-
313 sensory regions of the adult rosette. These observations suggest a complex
314 mechanism for ion regulation throughout the zebrafish olfactory epithelium, involving
315 region-specific roles for different ionocyte types.

316 **Pairing of NaR-like and HR-like ionocytes may extend functionality**

317 The pairing of NaR-like and HR-like ionocytes in the olfactory epithelium
318 appears robust. The cells are connected to each other by specialised tight junctions
319 and are dependent on Notch signalling for survival. The existence of ionocytes in
320 pairs or complexes is well established, for example in the gills and skin of
321 stenohaline saltwater fish [42,43], euryhaline fish adapted to seawater [19,44–48],
322 and in stenohaline freshwater teleosts [49]. Pairs were also seen in the skin of the
323 euryhaline medaka, when reared in freshwater [50]. In these cases, however, one
324 member of the pair was termed an accessory cell. Although accessory cells have
325 some features of ionocytes – they are mitochondria-rich, for example – they have
326 been considered to be immature or dormant [42] or specific to seawater fish [45].
327 The data here, and in the neuromast [17], indicate that both members of a pair in the
328 freshwater zebrafish are *bona fide* ionocytes.

329 The conservation of architecture across evolutionarily diverse fish species
330 suggests a functional advantage in using pairs. One consequence of ionocyte pairing
331 is the creation of a paracellular pathway that is regulated by both members of the
332 pair. In the olfactory epithelium, the apical half of the NaR-like cell wraps around the
333 HR-like cell, forming a paracellular pathway in the space between the two cells. Both
334 members of the pair extend from just above the basal lamina to the surface within
335 the sensory zone. Here, it is possible that the ionocyte pairs directly regulate ion
336 concentration within the mucus and epithelium to optimise olfactory transduction. For
337 example, one possible role could be to enable uptake of Cl^- after a neuronal
338 signalling event, with apical uptake and basal secretion of Na^+ by NaR-like and HR-
339 like ionocytes providing the driving force. This would supplement Cl^- uptake by
340 dendrites of the sensory neurons. NaR-like/HR-like ionocyte pairs are also found in

341 the zebrafish neuromast [17], which contains sensory hair cells that—like OSNs—
342 signal with a chloride efflux [51]. Thus, this specific pair may enable transport of ions
343 that is required for this mode of signalling.

344 NCC-like olfactory ionocytes are located in non-sensory regions 345 containing motile cilia

346 NCC-like ionocytes are strikingly different from NaR-like and HR-like
347 ionocytes in a number of respects. In the larval and adult olfactory epithelium, NCC-
348 like ionocytes appear to be restricted to non-sensory regions. Here, they are
349 interspersed among multiciliated cells, which contain motile cilia that drive water into
350 the olfactory pit [52,53]. By contrast, NCC ionocytes are absent from the zebrafish
351 neuromast, which lack motile cilia. A close association between ionocytes and motile
352 cilia has been observed in the skin of *Xenopus tropicalis*, where depletion of
353 ionocytes disrupts ciliary beating [54]. In the mammalian airway, ciliary beat is
354 regulated by intracellular chloride levels [55,56]. These observations raise the
355 possibility that NCC-like ionocytes function specifically to influence ciliary beating in
356 the zebrafish olfactory epithelium, which in turn shapes the detection of odorants
357 [53].

358 Shared and unique properties of zebrafish olfactory ionocytes

359 In mammals, Foxi1^{+} ionocytes have been identified in various tissues
360 including the kidney [57], airway epithelium [58,59], inner ear [16], salivary gland [60]
361 and thymus [61]. These ionocytes, which are critical to function, display a number of
362 tissue-specific properties, including type of transporters expressed and morphology.
363 Tissue-specific gene expression in zebrafish ionocytes is illustrated by the larval
364 transcriptome: olfactory ionocytes cluster with olfactory epithelial cells, rather than
365 skin ionocytes. The clustering of ionocytes within their tissue of residency indicates

366 that they share a transcriptional signature with the cells they regulate. Some of these
367 genes are likely to code for adhesion molecules, which are highly enriched in all
368 ionocyte transcriptomes that we have analysed thus far. Other genes may be
369 involved in cell-cell communication and cell signalling pathways.

370 In summary, this study has yielded two unexpected features of ionocytes in
371 the zebrafish olfactory epithelium. Firstly, the epithelium contains pairs of NaR-
372 like/HR-like ionocytes, implying that synergy between these ionocyte types is
373 essential for maintaining ion balance. Secondly, NCC-like ionocytes are restricted to
374 non-sensory regions, implying a distinct function in the regulation of motile cilia.
375 Ionocytes thus have diverse roles in enabling optimal olfaction.

376 Materials and Methods

377 Zebrafish husbandry

378 Zebrafish strains used in this study were AB and ABTL strain wild types,
379 *nacre* (*mitfa*$^{-/-}$) [62], *oval* (*ift88*^{tz288b}) [63], *Tg(tp1bglobin:EGFP)*^{um14} [64],
380 *Tg(krtt1c19e:lyn-tdTomato)*^{sq16} [65], *Tg(dld:hist2h2l-EGFP)*^{psi84} [30], and *Tg(-*
381 *8.0cldnb:lyn-EGFP)*^{zf106Tg} [66]. Adult zebrafish were kept on a 10-hour dark/14-hour
382 light cycle at 28.5°C and spawned by pair-mating or marbling. Eggs were collected
383 and staged according to standard protocols, and raised either in 0.5× embryo E2
384 medium (7.5 mM NaCl, 0.25 mM KCl, 0.5 mM $MgSO_4$, 75 mM KH_2PO_4, 25 mM
385 Na_2HPO_4, 0.5 mM $CaCl_2$, 0.5 mg/L $NaHCO_3$, pH = 7.4) or 1× E3 medium (5 mM
386 NaCl, 0.17 mM KCl, 0.33 mM $CaCl_2$, 0.33 mM $MgSO_4$, with 0.0001% methylene blue
387 at early stages) at 28.5°C. Larvae were anaesthetised with 0.5 mM tricaine
388 methanesulfonate (MS222) at pH 7.

Dissection of adult olfactory organs

Adult ABTL wild-type strain zebrafish were culled on ice and fixed in 4% paraformaldehyde (PFA) in 1× phosphate-buffered saline (PBS) overnight at 4°C. Adult zebrafish were transferred to a SYLGARD 184-coated (Dow Corning) Petri dish containing PBS, and olfactory organs were dissected out using Dumont #5SF forceps (Fine Science Tools). Olfactory organs were washed in PBS before proceeding with staining protocols.

Single-cell RNA sequencing (scRNA-seq) analysis

Analysis was carried out on published datasets generated from dissected adult zebrafish olfactory organs [30]. All four PBS-treated datasets were downloaded with sratoolkit (version 3.1.1). Reads were de-multiplexed and aligned to version Ensembl GRCz11 (danRer11.Ens_106) of the zebrafish genome using the CellRanger (version 7.1.0) pipeline. Subsequent analysis of the UMI count matrix was performed using Seurat (version 5.1.0) [67–71] in R version 4.3.3. Initial quality control filtered out genes expressed in fewer than three cells and cells with fewer than 200 genes. Further quality control was performed to exclude cells with more than 20000 UMIs or more than 10% mitochondrial content. The four resulting Seurat objects were combined with the function *merge()*, and cluster markers were identified with the function *FindAllMarkers()*. Dimensional reduction was performed (UMAP), and final clusters were obtained with 30 dimensions and resolution of 0.5.

Daniocell data were downloaded from the taste/olfactory subset [34]; no additional processing or clustering was performed. Ionocytes were identified based on their expression of *foxi3b*. For solitary ionocytes, a dataset from larvae was used. Olfactory epithelial cells were subset based on cluster expressions of *ompb* and

413 *trpc2a/2b*. Solitary olfactory ionocytes were then identified and manually clustered
414 based on their *foxi3b* expression, using the function subset (object, subset = *foxi3b* >
415 0). Markers were then subsequently identified with the function *FindAllMarkers()*.
416 Feature plots for all datasets were made with the function *FeaturePlot_scCustom()*
417 from the package scCustomize.

418 Hybridization chain reaction RNA-fluorescence *in situ* hybridization 419 (HCR RNA-FISH)

420 HCR RNA-FISH was performed on 5 dpf stage *nacre* wild-type or
421 *Tg(tp1bglobin:EGFP)* transgenic larvae following "HCR RNA-FISH protocol for
422 whole-mount zebrafish embryos and larvae (*Danio rerio*)" provided by Molecular
423 Instruments or adapted with acetone-based permeabilization [17]. The probe sets
424 used in this project were *ceacam1*-B1 (accession #: NM_001113794), *trpv6*-B1 and
425 B2 (accession #: NM_001001849), *foxi3a*-B2 (accession #: NM_198917.2), *foxi3b*-
426 B3 and B4 (accession #: NM_198918), *slc12a10.2*-B1 (accession #:
427 NM_001045001.1), *slc4a1b*-B1 (accession #: NM_001168266.1), *slc9a3.2*-B4
428 (accession #: NM_001113479.1), *chrd*-B2 (accession #: NM_130973.3), and
429 *hepacam2*-B2 (accession #: NM_001245085.1). The amplifiers used were B1-488,
430 B1-647, B2-546, B2-594, B3-546, B3-647, and B4-488 (Molecular Instruments). All
431 samples were stored in PBS at 4°C before imaging. The above standard HCR RNA-
432 FISH protocol for larvae was modified for staining on dissected olfactory organs of
433 adult ABTL fish. The proteinase K treatment step was adjusted to incubation in 30
434 µg/ml of proteinase K for 30 minutes. The remainder of the protocol remained the
435 same.

436 Confocal imaging

437 Fixed zebrafish larvae and olfactory organs were mounted in 1–2% low
438 melting point (LMP) agarose in PBS in glass-bottomed dishes, with larvae mounted
439 in a dorsal view. Samples were imaged on either a Zeiss LSM 800 attached to an
440 upright microscope with a W Plan Apochromat 40×/1.0 DIC M27 water dipping
441 objective, a Zeiss LSM 880 Airyscan confocal microscope equipped with a Plan-
442 Apochromat 20×/0.8 M27 air objective, a Zeiss LSM 980 Airyscan2 confocal
443 microscope equipped with a Plan-Apochromat 10x/0.45 air objective and an LCI
444 Plan-Apochromat 40x/1.2 water objective acquired in Airyscan SR-4Y mode, or a
445 Nikon Ti2 Yokogawa CSU-W1 spinning disk head equipped with a Hamamatsu Orca
446 Fusion sCMOS. Objective lenses used on the Nikon microscope were CFI Apo LWD
447 40× WI 1.15 NA Lambda S and CFI Apo 20× WI 0.95 NA Lambda S. The laser lines
448 used on the Zeiss microscopes were 488, 561, 568, 633, and 647 nm. A Nikon
449 LUNV solid state laser launch was used for lasers 395/405, 488, 561 and 647 nm for
450 GFP/Alexa488, RFP/Alexa546, and Alexa647 respectively. Emission filters used on
451 the Nikon were 480/30, 535/30, 605/52. Nikon Elements Advanced Research
452 v5.41.02 (Nikon) was used for image acquisition.

453 **Lineage tracing**

454 *Tg(krtt1c19e:lyn-Tomato)*^{sq16} and *Tg(dld:hist2h2l-EGFP)*^{psi84} 3–5 dpf larvae
455 were anaesthetised with buffered MS222 up to 150 mg/L and mounted in glass
456 bottom dishes (Cellvis) using 0.8% low melting point agarose dissolved in DI water
457 supplemented with buffered MS222 (120 mg/L). Time lapses were acquired in a
458 Nikon Ti2 Yokogawa CSU-W1 spinning disk head equipped with a Hamamatsu Orca
459 Fusion sCMOS and CFI Apo LWD 40× WI 1.15 NA Lambda S objective. A Stage
460 Top Incubator (OkoLab) was used to keep the constant temperature of 28.5˚C and
461 85% humidity.

Serial-section electron microscopy (ssEM)

At 7 dpf, a larval zebrafish underwent aldehyde specimen fixation followed by heavy metal contrast staining for electron microscopy as described in [72]. The fish was embedded and cured in LX-112 resin, cut in 30nm thick sections using an automated tape collection ultramicrotome (ATUM) system [73] and mounted on silicon wafers (University Wafers, USA) for imaging. The image volume was obtained with a Zeiss multibeam scanning electron microscope (mSEM) equipped with 61 overlapping electron beams [74] following the procedure outlined in [75]. Rigid stitching was performed on raw microscope tiles by extracting SIFT features, with global optimization applied to smooth the results across each section, and elastic stitching used for sections with distortions. Low-resolution thumbnails were generated in real-time, matched with nearby sections, and refined using a spring mesh model to prepare the images for final alignment. We used SOFIMA [76] to obtain a precise alignment of the complete stack, following the procedures outlined previously [75]. Briefly, starting from roughly prealigned sections we computed an optical flow field between each pair of adjacent sections using 8x8 nm^2 EM images. The field vectors were estimated on a regular grid with 40 px spacing. We then modeled each section as an elastic spring mesh grid with edge sizes corresponding to the flow field vector spacing, and with additional 0-length springs representing the flow field vectors. We allowed the system to relax, regularizing the flow field and finding a solution balancing deformation of the original images and cross-sections alignment. We used the final state of the mesh to warp the images into alignment to obtain the 3D stack.

Sections were painted manually using VAST *Lite* version 1.4.1 [77]. 3D objects were exported as mesh files using the ‘vasttools.m’ MATLAB script in VAST

487 *Lite*, and processed in Fiji [78], using the 3D viewer plugin [79]. Empty sections in the
488 dataset (marking the position of knife changes) were removed in Blender
489 (blender.org).

490 Scanning electron microscopy (SEM)

491 Zebrafish larvae (*ift88*$^{-/-}$ homozygous mutants, lacking cilia) raised in 1× E3
492 medium were fixed at 4 dpf in 2.5% glutaraldehyde/0.1M sodium cacodylate buffer
493 overnight. Samples were washed in buffer, post-fixed in 2% aqueous osmium
494 tetroxide for 1 hour, and washed in buffer again. Samples were dehydrated through
495 a graded ethanol series (50, 75, 95, 100%), followed by 50:50 hexamethyldisilazane
496 (HMDS):ethanol, and then 100% HMDS. After removal of the HDMS, samples were
497 dried in a fume hood overnight. Samples were mounted onto a pin stub using a Leit-
498 C sticky tab and mounting putty, and gold-coated using an Edwards S150B sputter
499 coater. Samples were imaged in a Tescan Vega3 LMU Scanning Electron
500 Microscope (operating voltage, 15 kV) using a secondary electron detector.

501 Image processing, quantifications, and statistical analyses

502 Zeiss LSM 800 confocal images were subjected to Gaussian Blur 3D
503 processing (X:0, Y:0, Z:2) in Fiji. Zeiss LSM 880 Airyscan and LSM 980 Airyscan2
504 confocal images were subjected to Airyscan processing on Zen Blue 3.7 (Zeiss)
505 using “Auto” Airyscan processing parameters. Further processing (for example,
506 gamma correction, maximum intensity projections, and 3D rendering) was performed
507 in Fiji. For fluorescence intensity quantification, background subtraction was
508 performed with rolling ball radius of 50 pixels, and a ROI was drawn around each cell
509 of interest. Quantification was performed using the Analyze, Measure function in Fiji.

No image quantification was performed in gamma corrected images. Single channel confocal images may be presented with their grayscale values inverted.

Statistical analyses were carried out in GraphPad Prism 10. Datasets were considered normally distributed if they passed the Kolmogorov-Smirnov test. Subsequent statistical tests used are stated in the figure legends. Bars on graphs indicate mean ± standard error of the mean (S.E.M.), unless stated otherwise. P values are indicated as follows: $P > 0.05$ (not significant, ns), $P < 0.05$ (*), $P < 0.01$ (**), $P < 0.001$ (***), $P < 0.0001$ (****). Figures were prepared using Adobe Photoshop versions 25.9.0 and 25.11.0 and Adobe Illustrator versions 25.4.1 and 28.6.

Acknowledgements

We are grateful to Cynthia Shiyuan Chen for her help with scRNA-seq data analysis and to Nathalie Jurisch-Yaksi for generous discussion of the adult olfactory transcriptome datasets at early stages of this study. We thank Chris Hill for technical assistance with Scanning Electron Microscopy, which was carried out in the Cryo-Electron Microscopy Facility, University of Sheffield.

Author Contributions

Conceptualization: JP, TP, TTW, SJ; Data Analysis: JP, KYC, TTW; Funding acquisition: FE, JWL, TP, TTW, SJ; Investigation: JP, KYC, TTW, MDP, RS, JBW, YW, SW, MJ, SJ; Methodology: YW, SW, MJ, JWL, FE, VJ ; Resources: TP, TTW, JWL, FE, VJ, MJ, SJ; Supervision: JWL, FE, VJ, SJ, TTW, TP; Validation: JP;

Visualization: JP, NvH, TTW; Writing – original draft: JP, KYC, TTW, SJ; Writing – review and editing: SJ and TTW, with input from MDP, TP and KYC.

Competing Interests

The authors declare no competing interests.

Funding

Work in Kansas City was funded by a NIH (NIDCD) award 1R01DC015488-01A1 to T.P. and by institutional support from the Stowers Institute for Medical Research to T.P. Work in Singapore was funded by a Tier 2 grant (MOE-T2EP30121-0017) from the Ministry of Education, Singapore, to S.J. KYC was funded by an A*STAR Research Attachment Programme Ph.D. studentship (ARAP-2019-01-0014). Work in Sheffield was funded by a Wellcome Trust Investigator Award to T.T.W. (224355/Z/21/Z); imaging in Fig. 3 was performed in the University of Sheffield Wolfson Light Microscopy Facility, using equipment funded by the Medical Research Council (MRC) (MR/X012077/1). F.E. received funding from the National Institutes of Health (U19NS104653 and 1R01NS124017-01), and the Simons Foundation (SCGB 542973 and NC-GB-CULM-00003241-02). The funders had no role in study design, data collection and analysis, decision to publish, or preparation of the manuscript.

Data availability

Raw data underlying this manuscript can be accessed from the Stowers Original Data Repository at http://www.stowers.org/research/publications/libpb-2509.

Figures

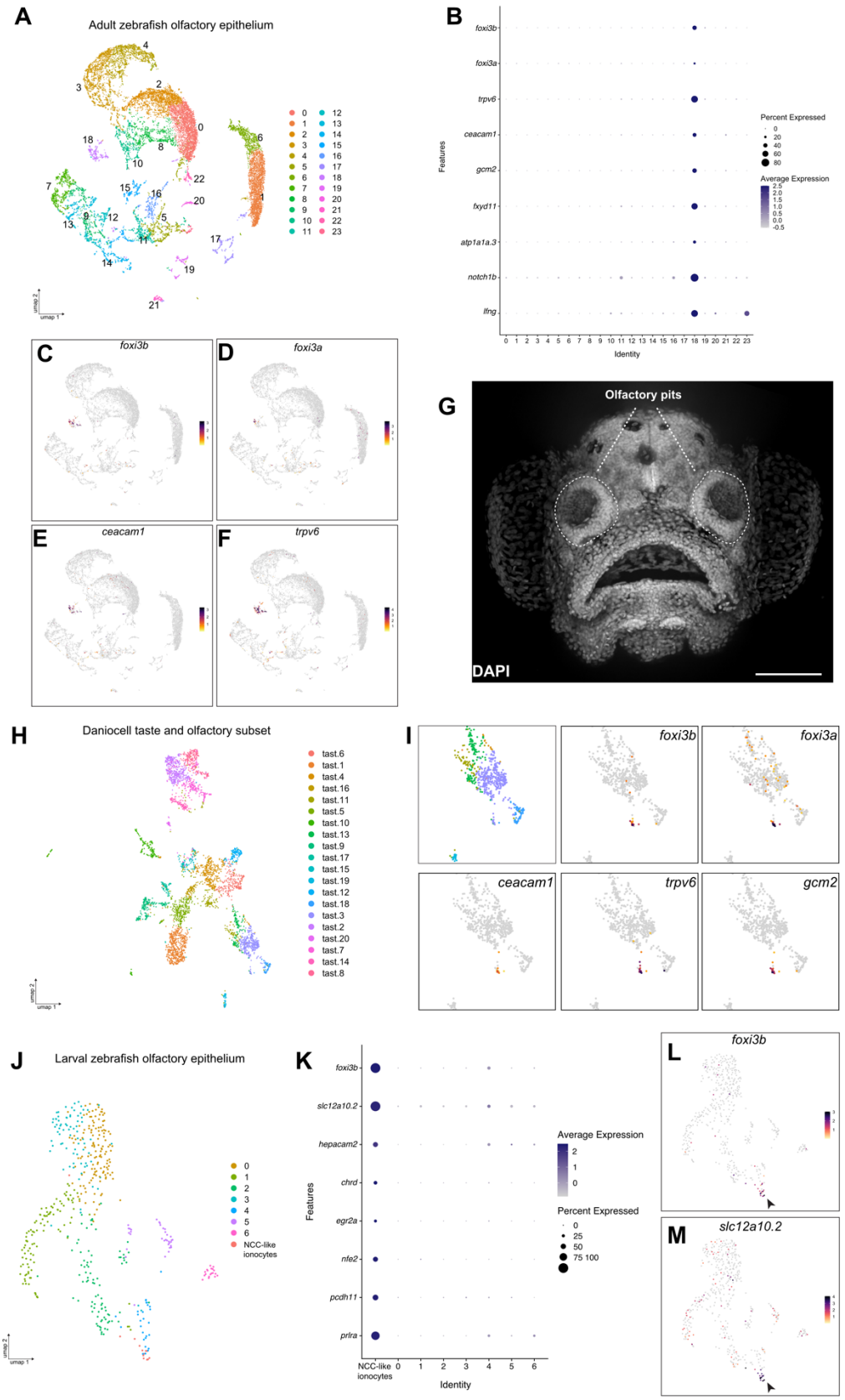
A
Adult zebrafish olfactory epithelium
B
foxi3b
foxi3a
trpv6
ceacam1
gcm2
fxyd11
atp1a1a.3
notch1b
lfng
Features
Identity
Percent Expressed
Average Expression
C
foxi3b
D
foxi3a
E
ceacam1
F
trpv6
G
Olfactory pits
DAPI
H
Daniocell taste and olfactory subset
I
foxi3b
foxi3a
ceacam1
trpv6
gcm2
J
Larval zebrafish olfactory epithelium
NCC-like ionocytes
K
slc12a10.2
hepacam2
chrd
egr2a
nfe2
pcdh11
prlra
L
M
slc12a10.2

553 **Figure 1. Single-cell RNA sequencing data analysis reveals expression of**
554 **classical ionocyte-marker genes in the zebrafish olfactory organ**
555 **(A)** UMAP plot showing 24 unannotated cell clusters (Identity) in the scRNA-seq
556 dataset generated from dissected adult zebrafish olfactory organs. **(B)** Dot plot of
557 data from B depicting several known ionocyte markers expressed in cluster 18. **(C)**
558 Feature plots for *foxi3b*, **(D)** *foxi3a*, **(E)** *ceacam1* and **(F)** *trpv6*. **(G)** Maximum
559 intensity projection of a 4 dpf larva stained with DAPI, frontal view shows the two
560 olfactory pits. Scale bar: 50 µm. **(H)** UMAP plot of taste/olfactory subset from
561 Daniocell [34]. **(I)** Zoomed in feature plots for the ionocyte markers *foxi3b, foxi3a,*
562 *ceacam1, trpv6* and *gcm2*. **(J)** UMAP plot of olfactory subset from [17]. **(K)** Dot plot
563 of data from J showing several NCC ionocyte markers in *foxi3b*$^{+}$ cells in the olfactory
564 epithelium. **(L)** Feature plots for *foxi3b* and **(M)** *slc12a10.2*.

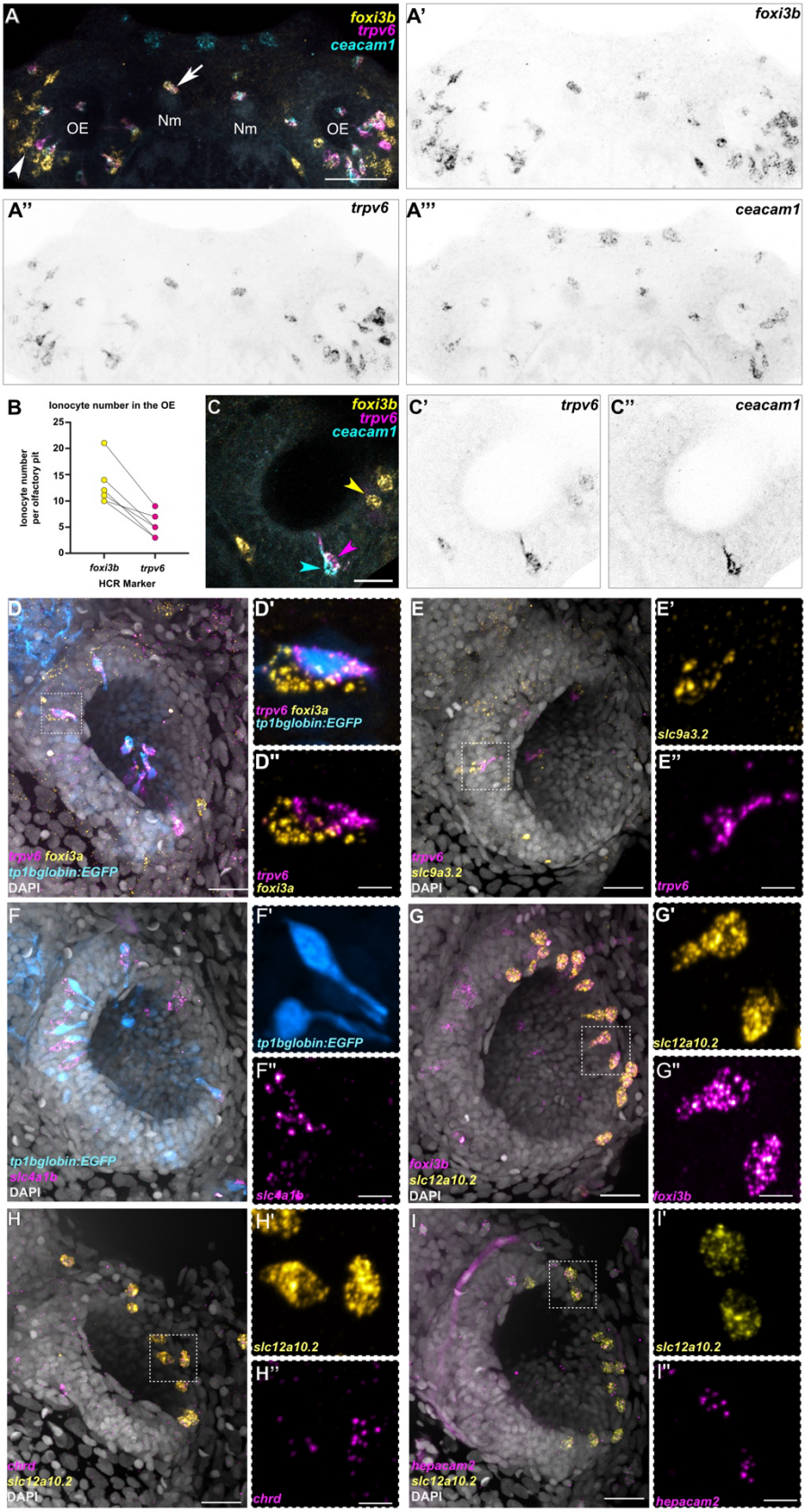

565

566 **Figure 2. The larval zebrafish olfactory epithelium contains three distinct**

567 **subtypes of ionocytes**

568 **(A–A’’’)** Maximum intensity projection of a confocal image of HCR RNA-FISH for
569 *foxi3b* **(A’)**, *trpv6* **(A’’)**, *ceacam1* **(A’’’)**, and merged signals **(A)** in the head of a 5 dpf
570 wild-type larva; dorsal view, anterior to the top. Scale bar: 50 µm. White arrowhead
571 marks an example of an olfactory ionocyte in the posterior-lateral region of the
572 olfactory pit with expression of *foxi3b*. White arrow marks an example neuromast
573 ionocyte with expression of all three selected genes. Abbreviations: OE; olfactory
574 epithelium, Nm; neuromast. **(B)** Numbers of *foxi3b*$^{+}$ ionocytes per olfactory pit in 5
575 dpf larvae raised in 0.5× E2 medium, of which also express *trpv6*. Connecting lines
576 indicate the same olfactory pit. **(C–C’’)** Confocal image of HCR RNA-FISH signals
577 for *trpv6* **(C’)**, *ceacam1* **(C’’)**, and merged signals **(C)** in the olfactory epithelium of a
578 5 dpf wild-type larva; dorsal view, anterior to the top, lateral to the right. Scale bar: 20
579 µm. Magenta and cyan arrowheads mark an example pair of ionocytes, with the
580 magenta arrowhead marking a strong *trpv6* and weak *foxi3b*-expressing cell, and the
581 cyan arrowhead marking a *ceacam1*$^{+}$ cell. Yellow arrowhead marks an example
582 solitary ionocyte, which has strong expression of *foxi3b* and weak expression of
583 *trpv6*. **(D–D’’)** HCR RNA-FISH for *foxi3a* (yellow) and *trpv6* (magenta), combined
584 with the Notch reporter *tp1bglobin:EGFP* (cyan) and DAPI stain (grey). **(E–E’’)** HCR
585 RNA-FISH for *slc9a3.2* (yellow) and *trpv6* (magenta) with DAPI stain (grey). **(F–F’’)**
586 HCR RNA-FISH for *slc4a1b* (magenta) combined with the Notch reporter
587 *tp1bglobin:EGFP* (cyan) and DAPI stain (grey). **(G–G’’)** Maximum intensity projection
588 of a HCR RNA-FISH for *slc12a10.2* (yellow) and *foxi3b* (magenta) with DAPI stain
589 (grey) shows solitary, NCC-like ionocytes in the olfactory epithelium. **(H–H’’)** HCR
590 RNA-FISH for *slc12a10.2* (yellow) and *chrd* (magenta) with DAPI stain (grey). **(I–I’’)**
591 HCR RNA-FISH for *slc12a10.2* (yellow) and *hepacam2* (magenta) with DAPI stain
592 (grey).

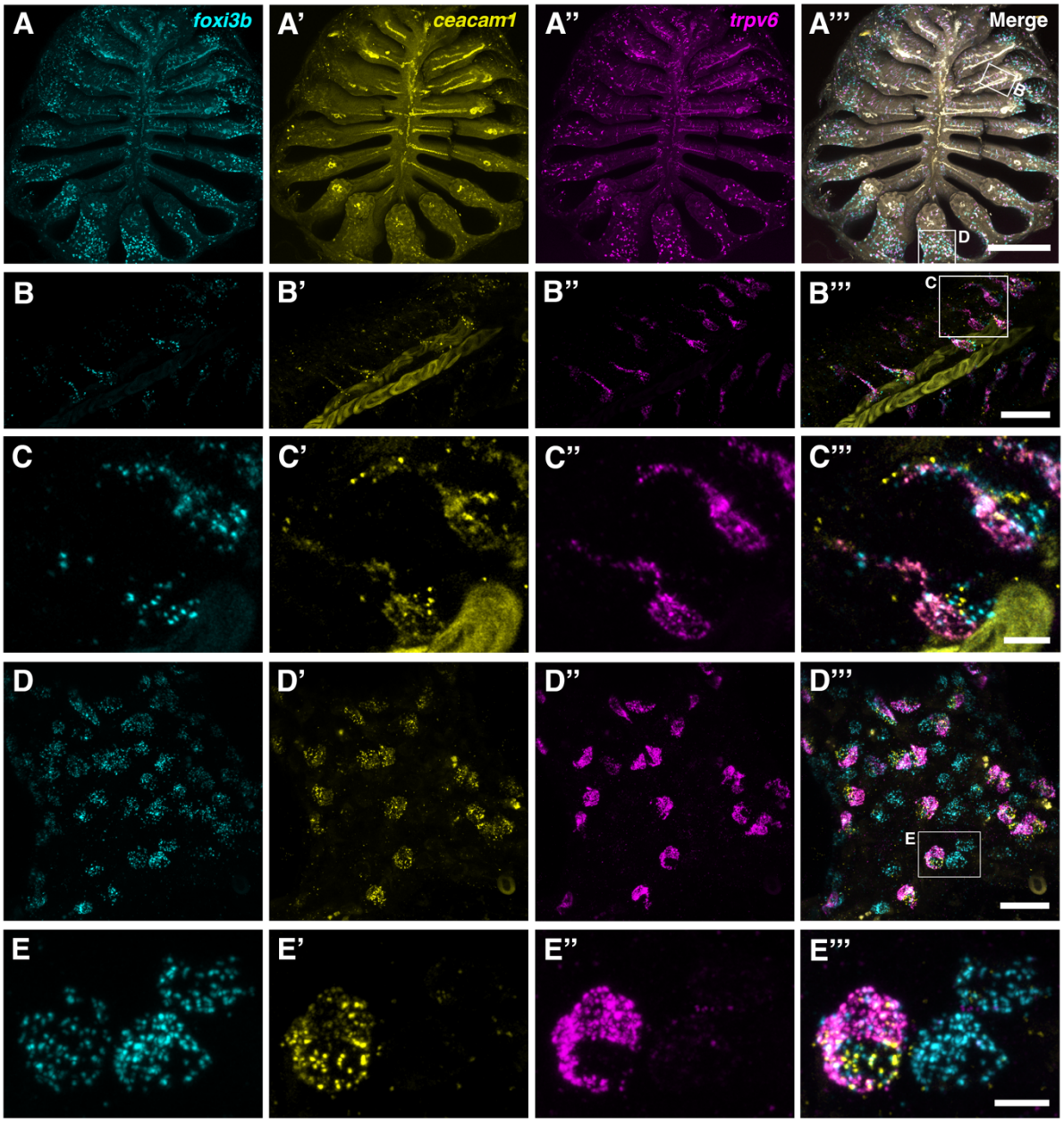

593

594 **Figure 3. The adult zebrafish olfactory epithelium contains three distinct**

595 **subtypes of ionocytes**

596 **(A–A'''')** Overview of a dissected adult olfactory rosette. Maximum intensity

597 projections of an Airyscan2 confocal image of HCR RNA-FISH for *foxi3b* **(A)**,

598 *ceacam1* **(A')**, *trpv6* **(A'')**, and merged signals **(A''')**. Scale bar: 200 µm. (**B–B'''**)

599 Enlargement of the boxed region 'B' in A''', within the central (sensory) zone of the

600 olfactory rosette. Maximum intensity projections of selected Airyscan2 confocal

slices; HCR RNA-FISH for *foxi3b* **(B)**, *ceacam1* **(B')**, *trpv6* **(B'')**, and merged signals **(B''')**. Pairs of elongated ionocytes with cell bodies located deep in the epithelium are visible. (The yellow stripe running through the image is autofluorescence from a blood vessel.) Scale bar: 20 µm. (**C–C'''**) Enlargement (maximum intensity projection of selected *z*-slices) of boxed region in B''', featuring two ionocyte pairs: HR-like ionocytes expressing *ceacam1* (yellow) and *foxi3b* (cyan), adjacent to NaR-like ionocytes expressing *trpv6* (magenta) and a low level of *ceacam1*. HCR RNA-FISH for *foxi3b* **(C)**, *ceacam1* **(C')**, *trpv6* **(C'')**, and merged signals **(C''')**. Scale bar: 5 µm. **(D–D''')** Enlargement of boxed region 'D' in A''', within the peripheral (non-sensory, multiciliated) zone of the olfactory rosette. Maximum intensity projections of selected Airyscan2 confocal *z*-slices; HCR RNA-FISH for *foxi3b* **(D)**, *ceacam1* **(D')**, *trpv6* **(D'')**, and merged signals **(D''')**. Both paired and solitary ionocytes are present. Scale bar: 20 µm. **(E–E''').** Enlargement (maximum intensity projection of selected *z*-slices) of the boxed region in D''', featuring one HR-like/NaR-like ionocyte pair, and two NCC-like ionocytes. An HR-like ionocyte, expressing *ceacam1* (yellow) and *foxi3b* (cyan), sits adjacent to an NaR-like ionocyte expressing *trpv6* (magenta) and a lower level of *ceacam1*. The NCC-like ionocytes express *foxi3b* (cyan) but not *ceacam1* or *trpv6*. Ionocytes near the periphery of the rosette were rounded in shape. Scale bar: 5 µm.

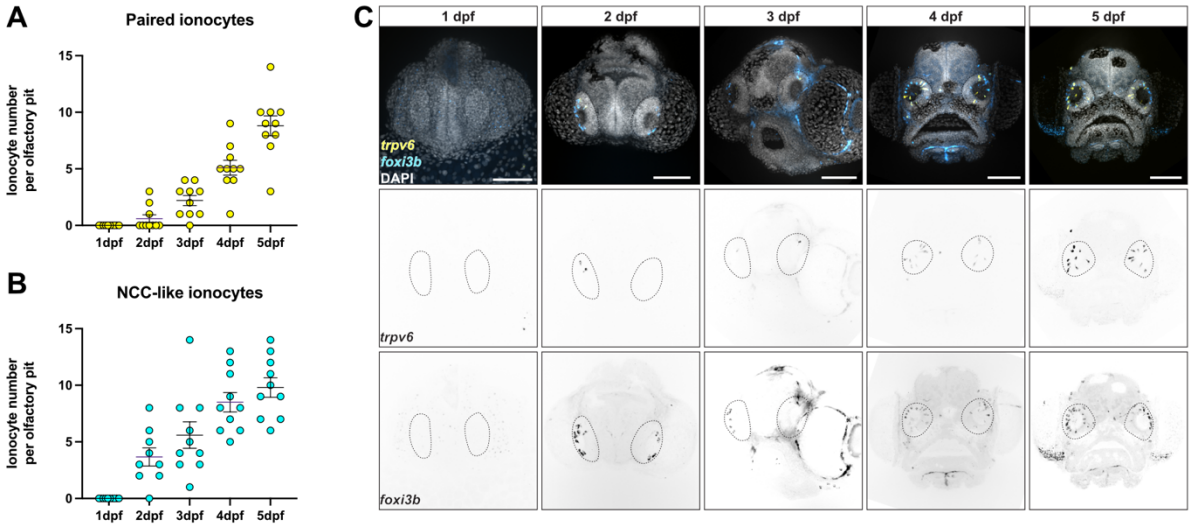

620

621 **Figure 4. The subtypes of olfactory ionocytes develop at different times**

622 **(A)** Developmental time course of NaR-/HR-like ionocyte pairs and **(B)** NCC-like

623 ionocytes from 1 to 5 dpf observed by confocal images of HCR RNA-FISH. **(C)**

624 Representative maximum intensity projection confocal images of HCR RNA-FISH for

625 *trpv6* (yellow) and *foxi3b* (cyan) with DAPI stain (grey) from A and B.

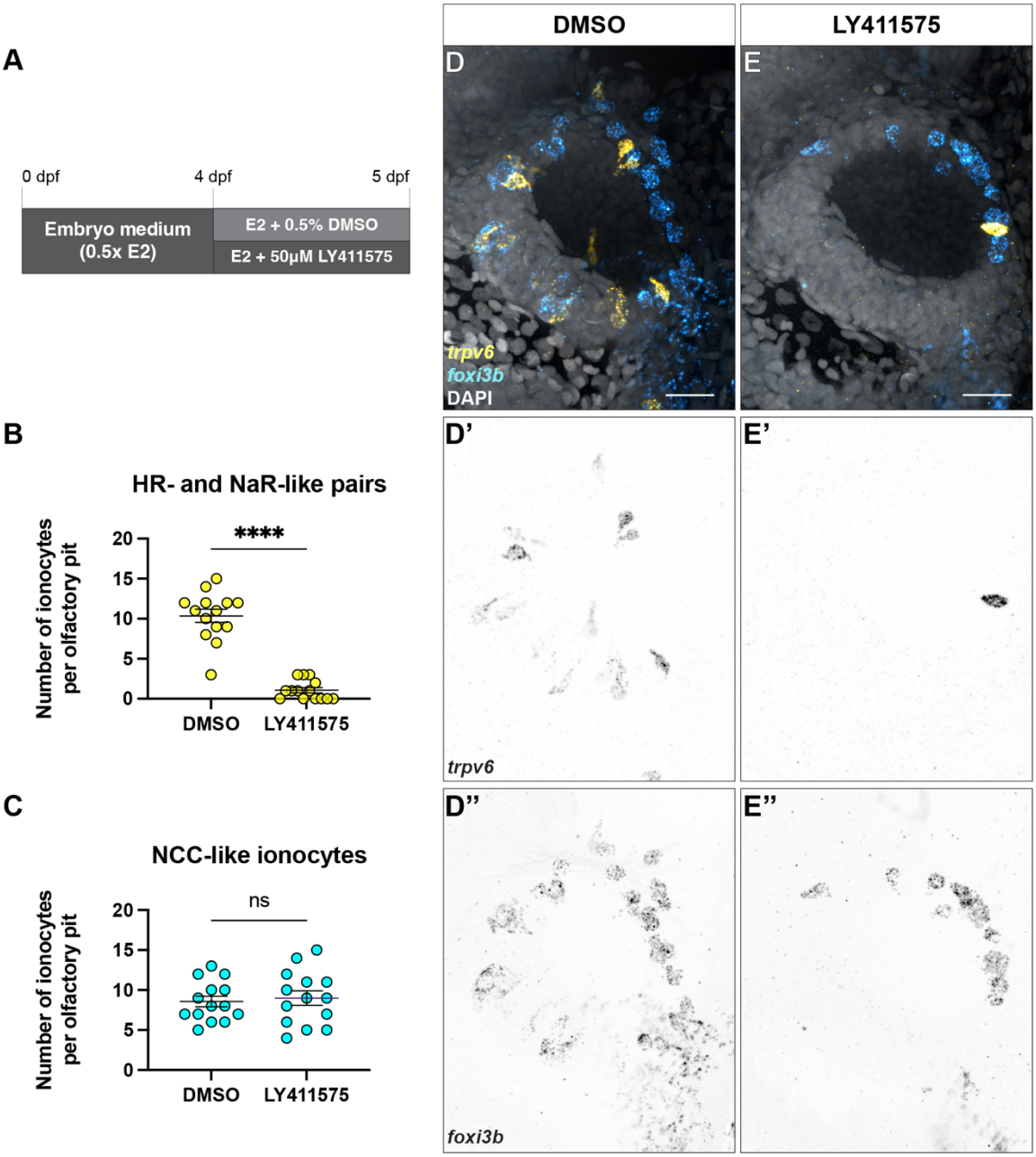

Figure 5. Notch signalling is required for paired ionocyte survival, but does not affect NCC-like ionocyte number

(A) Schematic of experimental design. **(B)** Number of NaR- and HR-like ionocyte pairs in DMSO controls and treated with the Notch inhibitor LY411575. Mann Whitney test ($P < 0.0001$). **(C)** Number of NCC-like ionocytes in DMSO controls and treated with the Notch inhibitor LY411575. Unpaired *t*-test ($P = 0.7070$). **(D–D'')** Representative maximum intensity projection confocal images of HCR RNA-FISH for

634 *trpv6* (yellow) and *foxi3b* (cyan) with DAPI stain (grey) in DMSO-treated and **(E–E'')**

635 LY411575-treated olfactory pits. *N* = 14 olfactory pits per condition. Scale bars: 20

636 µm.

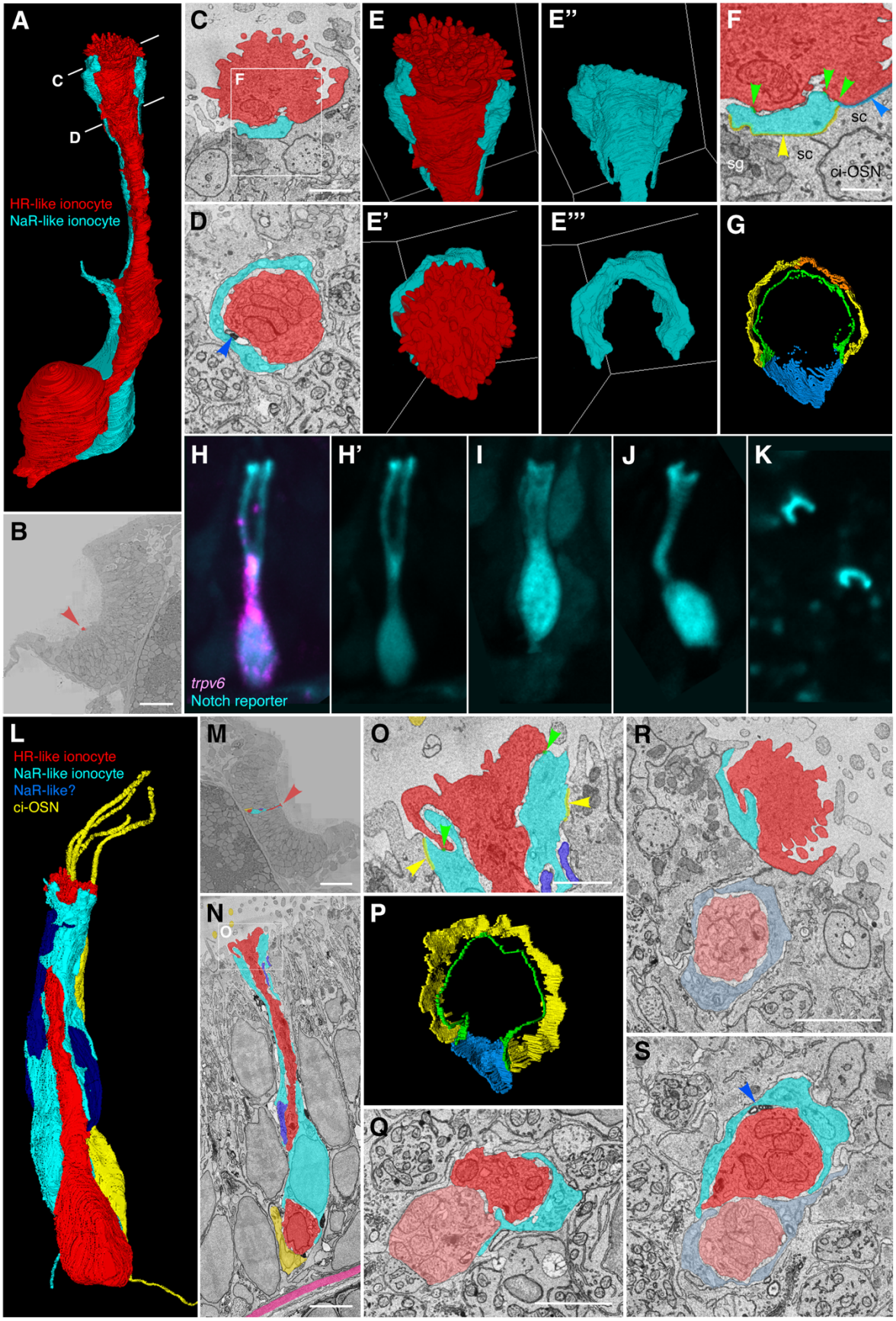
A
C
D
HR-like ionocyte
NaR-like ionocyte
B
C
F
D
E
E'
E''
E'''
F
sc
sc
sg
ci-OSN
G
H
H'
I
J
K
trpv6
Notch reporter
L
HR-like ionocyte
NaR-like ionocyte
NaR-like?
ci-OSN
M
N
O
P
Q
R
S

637

638 **Figure 6. Ultrastructure and 3D reconstruction of olfactory HR-like/NaR-like**
639 **ionocyte cell pairs and multicellular complexes in the wild-type zebrafish larva**

640 **(A–G)** Representative example of an ionocyte cell pair in the 7 dpf zebrafish larval
641 olfactory pit. The HR-like ionocyte is shown in red, with the NaR-like ionocyte in
642 cyan. **(A)** Volume-EM 3D reconstruction of the cell pair; see also Supplementary
643 Movie 6. **(B)** Location of the cell pair (red arrowhead) in the left olfactory pit (just
644 within the OSN zone). Coronal section; anterior to the top. **(C,D)** Sections at the
645 approximate levels shown in A. Blue arrowhead marks an electron-dense structure in
646 the extracellular space between the cell pair (see also S). **(E–E'''')** 3D
647 reconstructions of the apical part of the cell pair, showing the microvillous apical
648 knob of the HR-like ionocyte (red), which projects above the surrounding olfactory
649 supporting cells. The neck of the HR-like ionocyte is wrapped by a thin layer of
650 cytoplasm of the NaR-like cell (cyan). **(F,G)** Tight junctions (zonulae occludentes) of
651 the ionocyte pair. **(F)** Enlargement of the box in C, showing colour-coded labelling of
652 the junctions. Green, shallow tight junction between the two ionocytes; yellow, deep
653 tight junction between NaR-like ionocyte and olfactory supporting cell; orange, deep
654 tight junction between NaR-like ionocyte and multiciliated cell; blue, deep tight
655 junction between HR-like ionocyte and olfactory supporting cell. **Abbreviations:** ci-
656 OSN, ciliated olfactory sensory neuron; sc, olfactory supporting cell; sg, secretory
657 granule. **(G)** 3D reconstruction of the tight junctions (top-down view); see also
658 Supplementary Movie 7.

659 **(H–K)** Examples of NaR-like olfactory ionocytes in a live 5 dpf embryo, labelled by
660 EGFP (cyan) in the Notch reporter line *Tg(tp1bglob:EGFP)*. **(H)** Co-expression of
661 EGFP (Notch reporter; cyan) with HCR RNA-FISH for *trpv6* (magenta), confirming
662 the cell as an NaR-like ionocyte (see also Fig. 2E–E"). **(H',I–K)** EGFP (cyan) channel

663 only. **(I,J)** Additional examples in longitudinal view. **(K)** The apices of EGFP+ cells
664 (NaR-like ionocytes) appear as crescents in a top-down view.

665 **(L–S)** Examples of three- and four-cell ionocyte complexes in the wild-type zebrafish
666 olfactory epithelium at 7 dpf. **(L–P)** Example of a 3-cell complex, consisting of an
667 HR-like ionocyte (red), NaR-like ionocyte (cyan), and possible second NaR-like
668 ionocyte (dark blue). A nearby ciliated OSN (yellow) is included for context. **(L)** 3D
669 reconstruction of the ionocyte complex and ciliated OSN; see also Supplementary
670 Movie 8. **(M)** Location of the cells in the OSN zone of the right-hand olfactory pit (red
671 arrowhead). Coronal section. **(N)** Longitudinal section through the complex, showing
672 close association between the HR-like ionocyte (red) and the ciliated OSN (yellow) at
673 the base, and location relative to the basal lamina (pink). **(O)** Enlargement of the box
674 in C, showing colour-coded labelling of the tight junctions of the HR-like (red) and
675 NaR-like (cyan) cells (colour code as in F). **(P)** 3D reconstruction of the tight
676 junctions of the HR-like (red) and NaR-like (cyan) cells (top-down view; compare to
677 G; see also Supplementary Movie 9). **(Q)** Example section through a three-cell
678 complex consisting of an HR-like cell (red), an NaR-like cell (cyan), and possible
679 second HR-like cell (pink). **(R,S)** Example sections through a four-cell complex
680 consisting of two HR-like/NaR-like pairs. The cell pairs are separate at their apices
681 (R), but are closely associated beneath the epithelial surface (S). Blue arrowhead in
682 S marks electron-dense structures between the ionocytes.

683 **Scale bars: B**, 20 μm; **C**; 1 μm (applies to **D–E'''**, **G**); **F**, 0.5 μm; **M**, 20 μm; **N**, 3 μm;
684 **O**, 1 μm (applies to **P**); **Q**, 2 μm; **R**, 2 μm (applies to **S**).

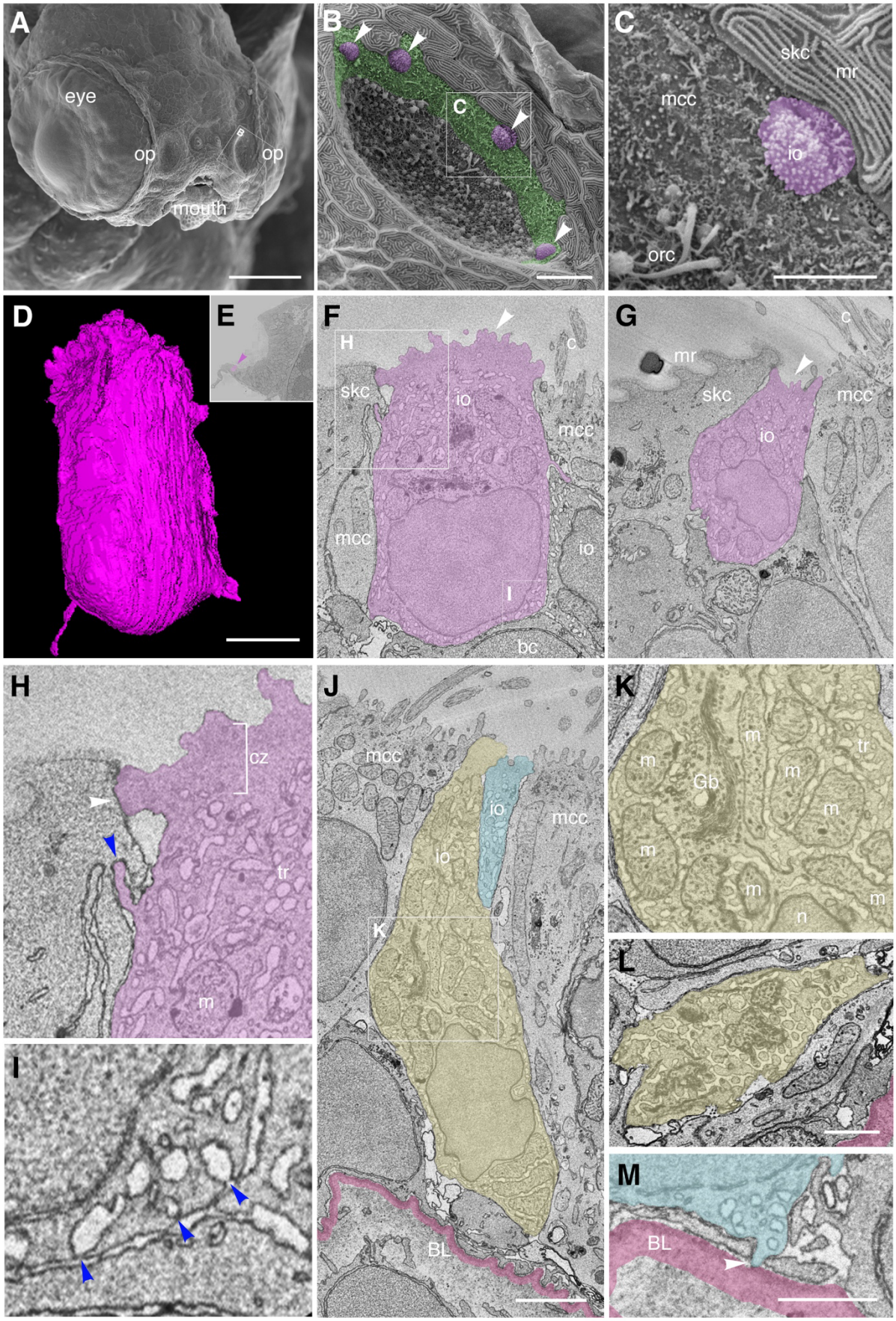
A
eye
op
op
mouth
B
C
C
skc
mr
mcc
io
orc
D
E
F
H
skc
io
c
mcc
mcc
io
I
bc
G
c
mr
skc
mcc
io
H
cz
tr
m
J
mcc
io
io
mcc
K
BL
K
m
tr
m
Gb
m
m
m
m
m
n
L
M
BL

685

686 **Figure 7. Ultrastructure and 3D reconstruction of NCC-like olfactory ionocytes**
687 **in the non-sensory multiciliated cell zone of the zebrafish olfactory pit**
688 **(A–C)** Scanning electron micrographs of an *ift88*$^{-/-}$ zebrafish mutant embryo at 4 dpf.
689 **(A)** Whole head showing location of the two olfactory pits (op). **(B)** Enlargement of
690 the left-hand olfactory pit, boxed in A. The rounded apical surfaces of four ionocytes
691 (presumed NCC-like) are highlighted in magenta (arrowheads). The peripheral zone
692 of non-sensory multiciliated cells (mcc) is highlighted in green. (All olfactory cilia are
693 missing in the *ift88*$^{-/-}$ mutant, allowing visualization of the apical surface of cells in the
694 pit.) **(C)** Enlargement of the boxed region in **B**. An ionocyte (magenta) sits in the
695 MCC zone, in contact with a skin cell with microridges (top right). The rods of two or
696 three olfactory rod cells are also visible (bottom left; see also Fig. 3I in [80]) .

697 **(D–M)** Ultrastructure and 3D reconstruction of ionocytes in the non-sensory
698 multiciliated zone of the olfactory pit in a wild-type zebrafish larva at 7 dpf. **(D)** 3D
699 reconstruction of a presumed NCC-like ionocyte, showing the microvillous apical
700 surface. **(E)** Location of the ionocyte in D (magenta; arrowhead) at the lateral edge of
701 the left olfactory pit. Coronal section. **(F,G)** Selected sections through the ionocyte
702 shown in D, highlighted in magenta. The ionocyte makes contact with at least four
703 other cell types: apically, with a skin cell on one side and a multiciliated cell on the
704 other; basolaterally, with multiciliated cells, a basal cell, and another ionocyte. The
705 microvillous apical surface is rounded in one area (F, arrowhead) but also forms a
706 pit-like structure (G, arrowhead) in the same cell. **(H)** Enlargement of the boxed
707 region in F (top left), highlighting tight junctional contact (white arrowhead) and
708 interdigitation (blue arrowhead) between the ionocyte and a neighbouring skin cell.
709 **(I)** Enlargement of the boxed region in F (bottom right), showing that pores where the
710 tubular reticulum meets the plasma membrane are covered by a thin electron-dense

structure (blue arrowheads). **(J)** Two examples of more elongated ionocytes highlighted in yellow and blue, with their apices sitting between multiciliated cells. **(K)** Enlargement of the boxed region in J, showing mitochondria-rich cytoplasm, Golgi apparatus and extensive tubular reticulum. **(L)** Section through the base of the yellow cell in J, showing the tubular reticulum. **(M)** An end-foot (arrowhead) of the blue ionocyte in J makes direct contact with the basal lamina (pink).

Abbreviations: bc, basal cell; BL, basal lamina (pink); c, cilia of multiciliated cell; cz, cortical zone (free of mitochondria; bracketed in H); Gb, Golgi body; io, presumed NCC-like ionocyte; m, mitochondrion; mcc, multiciliated cell; mr, microridges on skin cell; n, cell nucleus; op, olfactory pit; orc, olfactory rod cell (apical rods visible); skc, skin cell; tr, tubular reticulum.

Scale bars: A, 100 µm; **B**, 10 µm; **C**, 5 µm; **D**, 2 µm (applies to **F, G**); **J**; 2 µm; **L**, 1 µm; **M**, 1 µm.

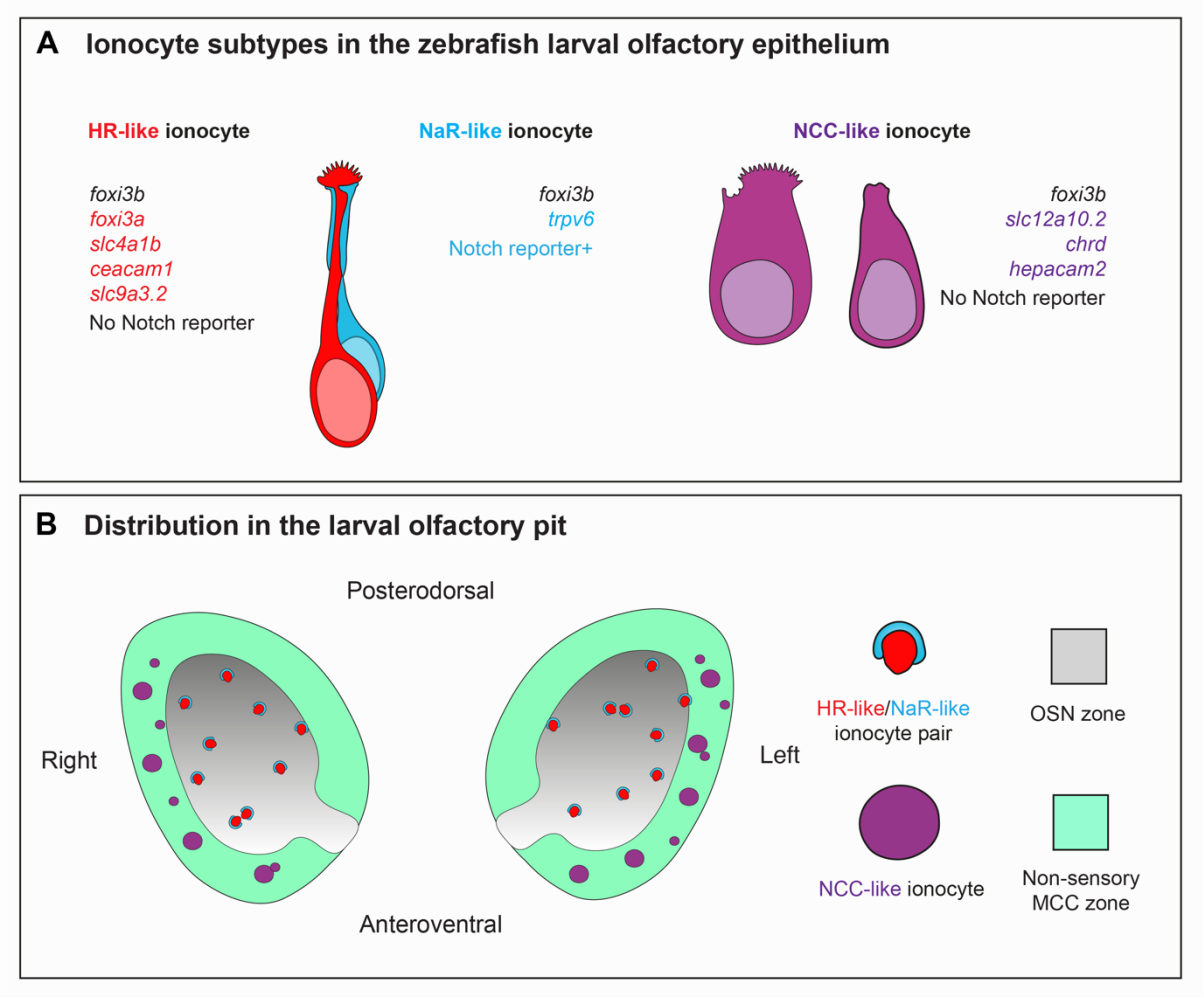

725

726 **Figure 8. Ionocytes in the zebrafish larval olfactory epithelium**

727 **(A)** Schematic of HR- and NaR-like ionocyte pairs and NCC-like ionocytes in the
728 zebrafish larval olfactory epithelium and their gene expression characterised in this
729 study. The NCC-like cells have variable morphologies, some with a rounded
730 microvillous apical surface. **(B)** Schematic showing distribution of ionocytes in the
731 zebrafish larval olfactory pit (viewed from the front; not to scale). Abbreviations:
732 MCC, multiciliated cell; OSN, olfactory sensory neuron.

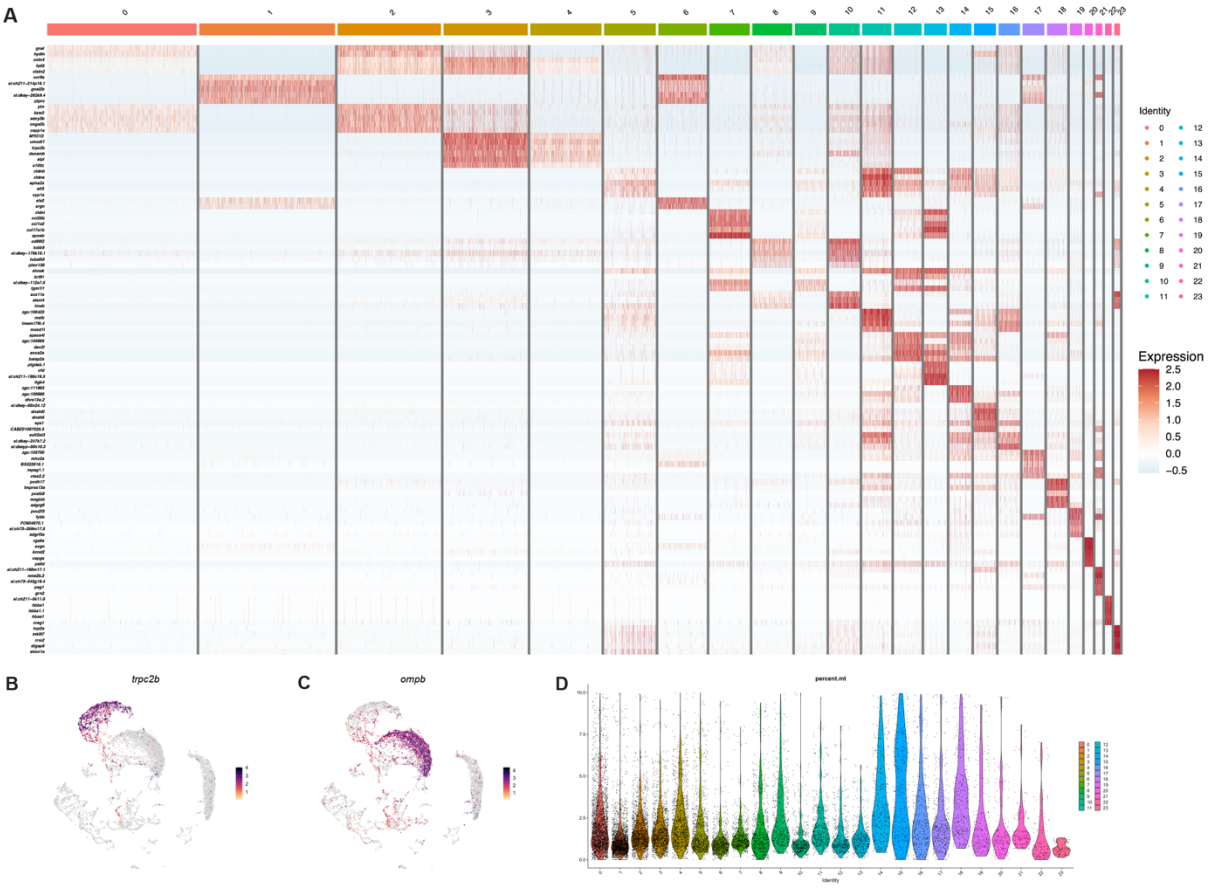

Figure S1, related to Figure 1

(A) Heatmap showing top 5 highest expressing genes based on LogFC on the clusters obtained in the dataset from dissected adult zebrafish olfactory organs. **(B)** Feature plots of *trpc2b* and **(C)** *ompb.* **(D)** Violin plot showing the percentage of mitochondrial genes in the dataset.

741 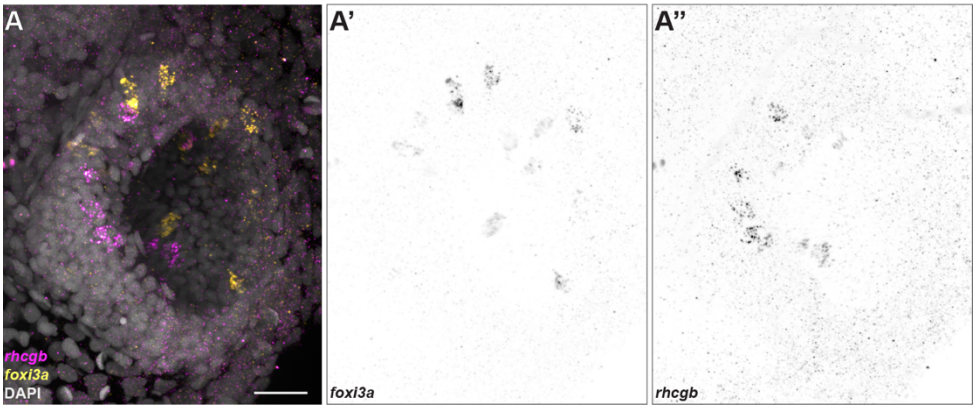

742 **Figure S2, related to Figure 2**

743 **(A)** Maximum intensity projection of a confocal image showing HCR RNA-FISH
744 signals for *foxi3a* (yellow) and *rhcgb* (magenta) with DAPI stain (grey). **(A')** Individual
745 channels for *foxi3a* and **(A'')** *rhcgb*. Scale bar: 20 µm.

746

747

748

749

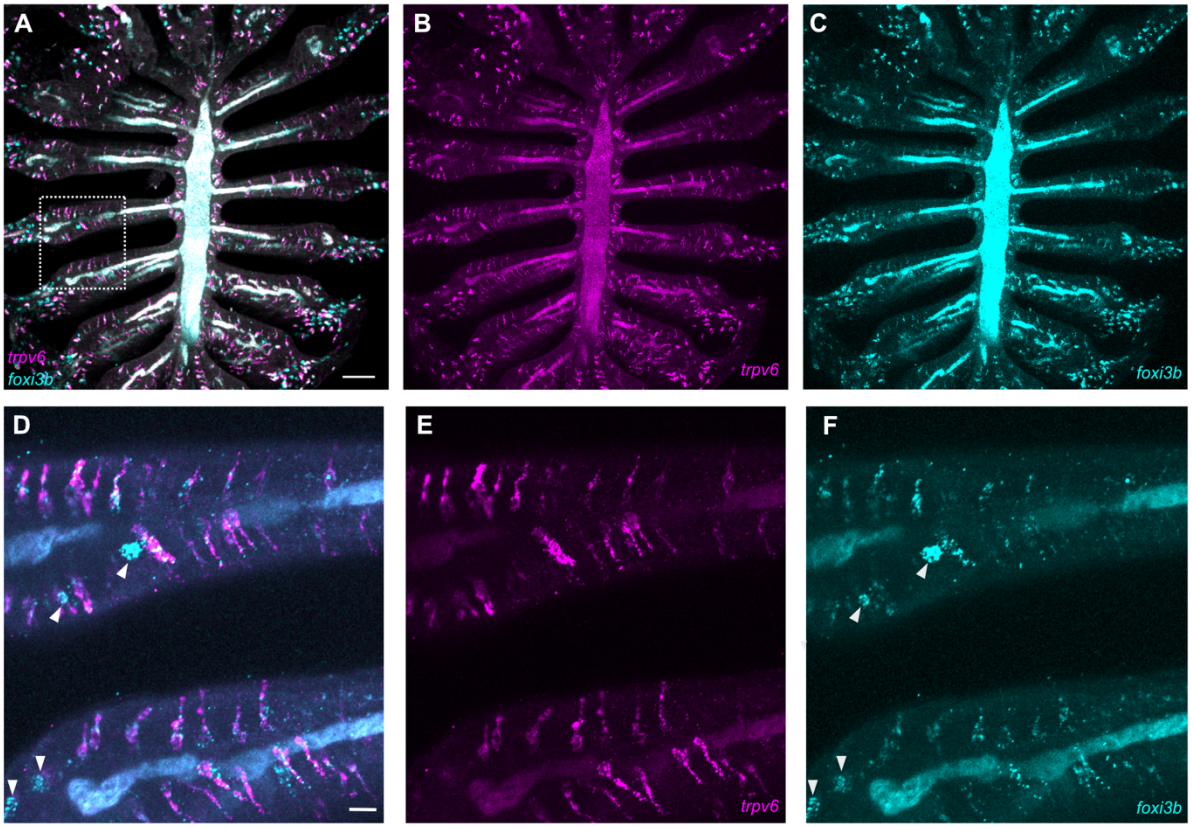

750

751 **Figure S3, related to Figure 3**

752 **(A-C)** Overview of an adult olfactory rosette, showing expression of *trpv6* **(B)** and
753 *foxi3b* **(C)**. **(D-F)** High magnification view of the region outlined in panel A. The
754 arrowheads indicate solitary NCC-like ionocytes, which express *foxi3b* and have a
755 rounded shape. These are distinct from elongated pairs of cells that express either
756 *foxi3b* or *trpv6*. Scale bar: 50 µm in panel A, 20 µm in panel D.

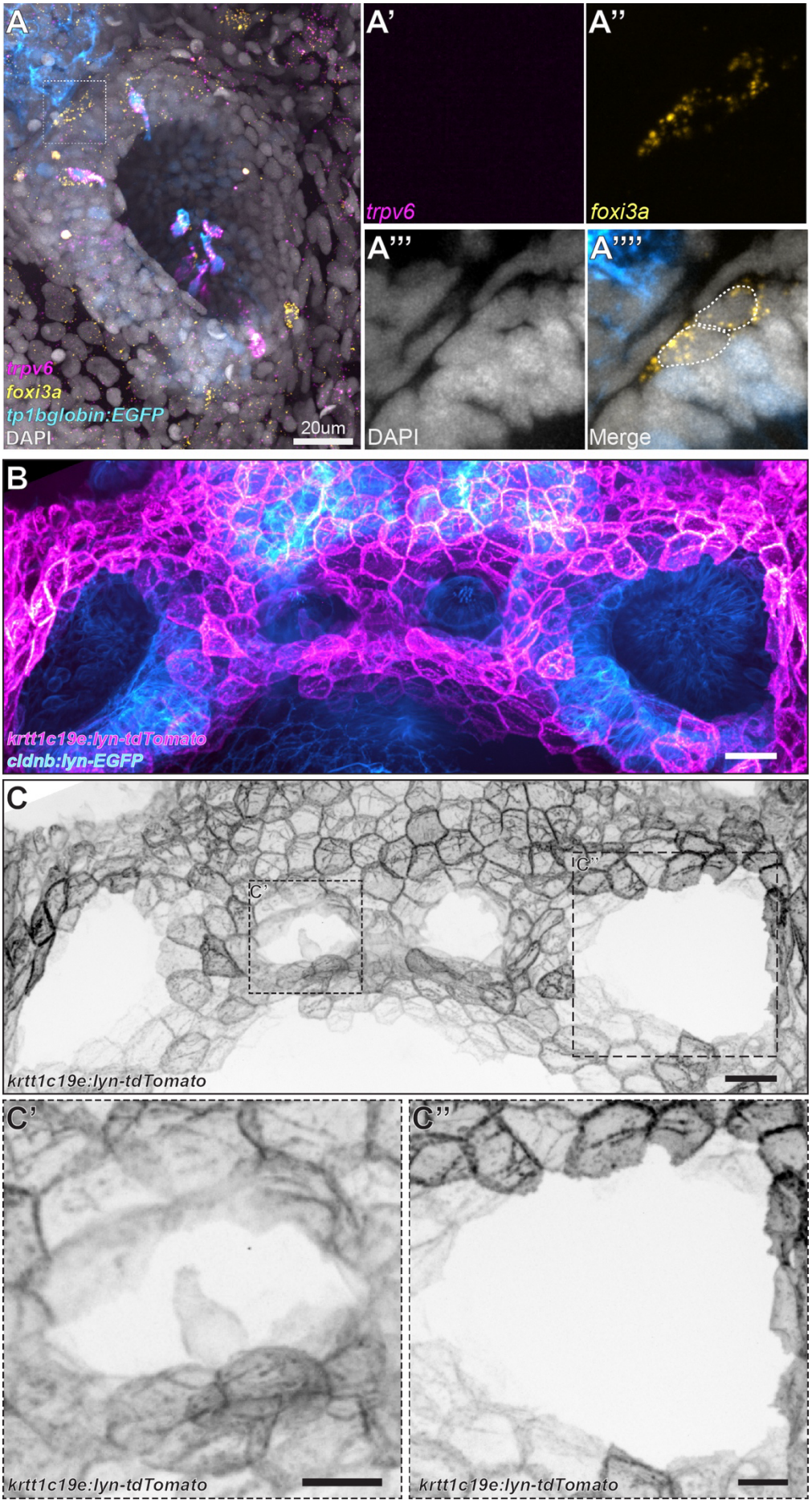
A
trpv6
foxi3a
tp1bglobin:EGFP
DAPI
20um
A'
trpv6
A''
foxi3a
A'''
DAPI
A''''
Merge
B
krtt1c19e:lyn-tdTomato
cldnb:lyn-EGFP
C
C'
C''
krtt1c19e:lyn-tdTomato
C'
krtt1c19e:lyn-tdTomato
C''
krtt1c19e:lyn-tdTomato

757

Figure S4, related to Figure 4

(A–A’’’’) *foxi3a+* cells (yellow) at the edge of an olfactory pit, as shown by HCR RNA-FISH. **(B)** Maximum intensity projection of a confocal image from *Tg(-8.0cldnb:lyn-EGFP)*^{zf106Tg}*;Tg(krtt1c19e:lyn-tdTomato)*^{sq16} transgenic larva shows a pair of Nm ionocytes in the neuromast, but no tdTomato^{+} cells in the olfactory pit. **(C)** Single channel image of *krtt1c19e:lyn-tdTomato*. **(C’)** Enlargement of a neuromast containing tdTomato^{+} Nm ionocytes. **(C’’)** Enlargement of an olfactory pit containing no tdTomato^{+} cells.

766 # Supplementary Material

767 **Supplementary Table 1. Differentially expressed genes in dissected adult**
768 **zebrafish olfactory organ scRNA-seq dataset.** This spreadsheet contains the
769 differentially expressed gene list (cluster markers) of olfactory cell types from the
770 integrated adult dataset via Seurat::FindAllMarkers function with default parameters.
771 Ionocytes are on cluster 18.

772 **Supplementary Table 2. Differentially expressed genes in larval 5 dpf olfactory**
773 **cell subset.** This spreadsheet contains the differentially expressed gene list (cluster
774 markers) of olfactory cell types from the subsetted larval dataset via
775 Seurat::FindAllMarkers function with default parameters.

776 **Movie 1. 3D rendering of an embryonic olfactory pit depicting HR- and NaR-like**
777 **ionocytes.** HCR RNA-FISH for *trpv6* (magenta) and *foxi3a* (yellow), combined with
778 the Notch reporter *tp1bglobin:EGFP* (cyan), shows spatial distribution of ionocyte
779 pairs in the larval 5 dpf olfactory pit. Initial image is a frontal view of the left olfactory
780 pit, with dorsal to the top and lateral to the right.

781 **Movie 2. 3D rendering of an embryonic olfactory pit showing NCC-like**
782 **ionocytes.** HCR RNA-FISH for *slc12a10.2* (yellow) and *foxi3b* (magenta), combined
783 with the Notch reporter *tp1bglobin:EGFP* (cyan), showing the spatial distribution of
784 ionocyte pairs in the larval 5 dpf olfactory pit. Initial image is a frontal view of the left
785 olfactory pit, with dorsal to the top and lateral to the right.

786 **Movie 3. New olfactory ionocytes do not express skin transgenes.** Time lapse
787 from *Tg(-8.0cldnb:lyn-EGFP)*^{zf106Tg}*;Tg(krtt1c19e:lyn-tdTomato)*^{sq16} transgenic

788 zebrafish larva showing pairs of tdTomato^{+} Nm ionocytes (arrow, middle panel)
789 invading neuromasts, but no positive cells in the olfactory epithelium.

790 **Movie 4. Differentiation of ionocyte pairs in a larval olfactory pit and**
791 **neuromast.** Time lapse from a 3 dpf transgenic zebrafishlarva (*Tg(dld:hist2h2l-*
792 *EGFP)^{psi84}*) showing a pair of ionocytes (cyan and yellow dots; visible at the start of
793 the recording) invading the neuromast. At ~90 hours ionocytes are visible in the
794 olfactory pit (red and cyan dots). No invasion was detected.

795 **Movie 5. Ionocyte pair development in a larval olfactory pit.** Time lapse from a 3
796 dpf transgenic zebrafish larva (*Tg(dld:hist2h2l-EGFP)^{psi84}*) showing the appearance
797 of a pair of olfactory ionocytes (red and cyan dots). The pair is visible at
798 approximately 85 hours, and move around together.

799 **Movie 6. 3D reconstruction of an HR-like/NaR-like ionocyte pair from a 7 dpf**
800 **wild-type olfactory pit.** 360° rotation of Fig. 6A. Red, HR-like cell; cyan, NaR-like
801 cell.

802 **Movie 7. 3D reconstruction of the tight junctions of an HR-like/NaR-like**
803 **ionocyte pair.** 360° rotation of Fig. 6G; compare to Movie 9. Green, shallow tight
804 junction between the two ionocytes; yellow, deep tight junction between NaR-like
805 ionocyte and olfactory supporting cell; orange, deep tight junction between NaR-like
806 ionocyte and multiciliated cell; blue, deep tight junction between HR-like ionocyte
807 and olfactory supporting cell.

808 **Movie 8. 3D reconstruction of a 3-cell ionocyte complex from a 7 dpf wild-type**
809 **olfactory pit.** 360° rotation of Fig. 6L. Red, HR-like cell; cyan, NaR-like cell; dark

810 blue, possible second NaR-like cell; yellow, ciliated OSN (not part of the ionocyte
811 complex, but included for context and scale).

812 **Movie 9. 3D reconstruction of the tight junctions between the HR-like (red) and**
813 **NaR-like (cyan) ionocytes in Fig. 6L.** 360° rotation of Fig. 6P; compare to Movie 7.
814 Green, shallow tight junction between the two ionocytes; yellow, deep tight junction
815 between NaR-like ionocyte (cyan) and olfactory supporting cell; blue, deep tight
816 junction between HR-like ionocyte (red) and olfactory supporting cell.

References

1. Kleene SJ. Origin of the chloride current in olfactory transduction. Neuron. 1993;11: 123–132. doi:10.1016/0896-6273(93)90276-w

2. Reuter D, Zierold K, Schröder WH, Frings S. A depolarizing chloride current contributes to chemoelectrical transduction in olfactory sensory neurons in situ. J Neurosci : Off J Soc Neurosci. 1998;18: 6623–30.

3. Kaneko H, Putzier I, Frings S, Kaupp UB, Gensch T. Chloride accumulation in mammalian olfactory sensory neurons. The Journal of neuroscience : the official journal of the Society for Neuroscience. 2004;24: 7931–7938. doi:10.1523/jneurosci.2115-04.2004

4. Reisert J, Reingruber J. Ca2+-activated Cl− current ensures robust and reliable signal amplification in vertebrate olfactory receptor neurons. Proc Natl Acad Sci. 2019;116: 1053–1058. doi:10.1073/pnas.1816371116

5. Selvaraj S, Liu K, Robinson AM, Epstein VA, Conley DB, Kern RC, et al. In Vivo Determination of Mouse Olfactory Mucus Cation Concentrations in Normal and Inflammatory States. PLoS ONE. 2012;7: e39600. doi:10.1371/journal.pone.0039600

6. Spence R, Fatema MK, Reichard M, Huq KA, Wahab MA, Ahmed ZF, et al. The distribution and habitat preferences of the zebrafish in Bangladesh. J Fish Biol. 2006;69: 1435–1448. doi:10.1111/j.1095-8649.2006.01206.x

7. Friedrich RW, Habermann CJ, Laurent G. Multiplexing using synchrony in the zebrafish olfactory bulb. Nat Neurosci. 2004;7: 862–871. doi:10.1038/nn1292

8. Niessing J, Friedrich RW. Olfactory pattern classification by discrete neuronal network states. Nature. 2010;465: 47–52. doi:10.1038/nature08961

9. Hansen A, Zeiske E. Development of the olfactory organ in the zebrafish, Brachydanio rerio. J Comp Neurol. 1993;333: 289–300. doi:10.1002/cne.903330213

10. Hansen A, Zeiske E. The peripheral olfactory organ of the zebrafish, Danio rerio: an ultrastructural study. Chemical Senses. 1998;23: 39–48. Available: http://eutils.ncbi.nlm.nih.gov/entrez/eutils/elink.fcgi?dbfrom=pubmed&id=9530968&retmode=ref&cmd=prlinks

11. Saraiva LR, Ahuja G, Ivandic I, Syed AS, Marioni JC, Korsching SI, et al. Molecular and neuronal homology between the olfactory systems of zebrafish and mouse. Scientific reports. 2015;5: 11487. doi:10.1038/srep11487

12. Hwang P-P, Chou M-Y. Zebrafish as an animal model to study ion homeostasis. Pflügers Arch - Eur J Physiol. 2013;465: 1233–1247. doi:10.1007/s00424-013-1269-1

13. Guh Y-J, Lin C-H, Hwang P-P. Osmoregulation in zebrafish: ion transport mechanisms and functional regulation. EXCLI J. 2015;14: 627–659. doi:10.17179/excli2015-246

14. Casellas CP, Pleguezuelos-Manzano C, Rookmaaker MB, Verhaar MC, Clevers H. Transcriptomic profile comparison reveals conservation of ionocytes across multiple organs. Sci Rep. 2023;13: 3516. doi:10.1038/s41598-023-30603-1

15. Ualiyeva S, Lemire E, Wong C, Perniss A, Boyd AA, Avilés EC, et al. A nasal cell atlas reveals heterogeneity of tuft cells and their role in directing olfactory stem cell proliferation. Sci Immunol. 2024;9: eabq4341. doi:10.1126/sciimmunol.abq4341

16. Honda K, Kim SH, Kelly MC, Burns JC, Constance L, Li X, et al. Molecular architecture underlying fluid absorption by the developing inner ear. eLife. 2017;6: e26851. doi:10.7554/elife.26851

17. Peloggia J, Münch D, Meneses-Giles P, Romero-Carvajal A, Lush ME, Lawson ND, et al. Adaptive cell invasion maintains lateral line organ homeostasis in response to environmental changes. Dev Cell. 2021;56: 1296-1312.e7.

867 doi:10.1016/j.devcel.2021.03.027

868 18. Hwang P. Ultrastructural study on multicellular complex of chloride cells in

869 teleosts. Bull Inst Zool, Academia Sinica. 1988.

870 19. Cozzi RRF, Robertson GN, Spieker M, Claus LN, Zaparilla GMM, Garrow KL, et

871 al. Paracellular pathway remodeling enhances sodium secretion by teleost fish in

872 hypersaline environments. J Exp Biol. 2015;218: 1259–1269.

873 doi:10.1242/jeb.117317

874 20. Bertmar G. Labyrinth cells, a new cell type in vertebrate olfactory organs. Z für

875 Zellforsch Mikrosk Anat. 1972;132: 245–256. doi:10.1007/bf00307014

876 21. Ruzhinskaya NN, Gdovskii PA, Devitsina GV. Chloride Cells, A Constituent of

877 the Fish Olfactory Epithelium. J Evol Biochem Physiol. 2001;37: 89–94.

878 doi:10.1023/a:1017526204623

879 22. Ghosh SK. Histoanatomy and surface ultrastructure of the olfactory organ of the

880 freshwater tank goby, Glossogobius giuris (Hamilton, 1822). Fish Aquat Life.

881 2020;28: 141–148. doi:10.2478/aopf-2020-0017

882 23. Hsiao C-D, You M-S, Guh Y-J, Ma M, Jiang Y-J, Hwang P-P. A Positive

883 Regulatory Loop between foxi3a and foxi3b Is Essential for Specification and

884 Differentiation of Zebrafish Epidermal Ionocytes. PLoS ONE. 2007;2: e302.

885 doi:10.1371/journal.pone.0000302

886 24. Jänicke M, Carney TJ, Hammerschmidt M. Foxi3 transcription factors and Notch

887 signaling control the formation of skin ionocytes from epidermal precursors of the

888 zebrafish embryo. Dev Biol. 2007;307: 258–271. doi:10.1016/j.ydbio.2007.04.044

889 25. Hwang P-P. Ion uptake and acid secretion in zebrafish (Danio rerio). J Exp Biol.

890 2009;212: 1745–1752. doi:10.1242/jeb.026054

891 26. Pan T-C, Liao B-K, Huang C-J, Lin L-Y, Hwang P-P. Epithelial Ca2+ channel

892 expression and Ca2+ uptake in developing zebrafish. Am J Physiol-Regul, Integr
893 Comp Physiol. 2005;289: R1202–R1211. doi:10.1152/ajpregu.00816.2004
894 27. Kowalewski J, Paris T, Gonzalez C, Lelièvre E, Valencia LC, Boutrois M, et al.
895 Characterization of a member of the CEACAM protein family as a novel marker of
896 proton pump-rich ionocytes on the zebrafish epidermis. PLoS ONE. 2021;16:
897 e0254533. doi:10.1371/journal.pone.0254533
898 28. Wang Y-F, Tseng Y-C, Yan J-J, Hiroi J, Hwang P-P. Role of SLC12A10.2, a Na-
899 Cl cotransporter-like protein, in a Cl uptake mechanism in zebrafish (Danio rerio).
900 Am J Physiol-Regul, Integr Comp Physiol. 2009;296: R1650–R1660.
901 doi:10.1152/ajpregu.00119.2009
902 29. Shih S-W, Yan J-J, Lu S-W, Chuang Y-T, Lin H-W, Chou M-Y, et al. Molecular
903 Physiological Evidence for the Role of Na+-Cl− Co-Transporter in Branchial Na+
904 Uptake in Freshwater Teleosts. Int J Mol Sci. 2023;24: 6597.
905 doi:10.3390/ijms24076597
906 30. Kraus A, Huertas M, Ellis L, Boudinot P, Levraud J-P, Salinas I. Intranasal
907 delivery of SARS-CoV-2 spike protein is sufficient to cause olfactory damage,
908 inflammation and olfactory dysfunction in zebrafish. Brain, Behav, Immun. 2022;102:
909 341–359. doi:10.1016/j.bbi.2022.03.006
910 31. Saito K, Nakamura N, Ito Y, Hoshijima K, Esaki M, Zhao B, et al. Identification of
911 Zebrafish Fxyd11a Protein that is Highly Expressed in Ion-Transporting Epithelium of
912 the Gill and Skin and its Possible Role in Ion Homeostasis. Front Physiol. 2010;1:
913 129. doi:10.3389/fphys.2010.00129
914 32. Liao B-K, Chen R-D, Hwang P-P. Expression regulation of Na+-K+-ATPase α1-
915 subunit subtypes in zebrafish gill ionocytes. Am J Physiol-Regul, Integr Comp
916 Physiol. 2009;296: R1897–R1906. doi:10.1152/ajpregu.00029.2009

917 33. Peloggia J, Lush ME, Tsai Y-Y, Wood C, Piotrowski T. Environmental and
918 molecular control of tissue-specific ionocyte differentiation in zebrafish. bioRxiv.
919 2024; 2024.01.12.575421. doi:10.1101/2024.01.12.575421
920 34. Sur A, Wang Y, Capar P, Margolin G, Prochaska MK, Farrell JA. Single-cell
921 analysis of shared signatures and transcriptional diversity during zebrafish
922 development. Dev Cell. 2023;58: 3028-3047.e12. doi:10.1016/j.devcel.2023.11.001
923 35. Farrell JA, Wang Y, Riesenfeld SJ, Shekhar K, Regev A, Schier AF. Single-cell
924 reconstruction of developmental trajectories during zebrafish embryogenesis.
925 Science. 2018;360. doi:10.1126/science.aar3131
926 36. Trivedi V, Choi HMT, Fraser SE, Pierce NA. Multidimensional quantitative
927 analysis of mRNA expression within intact vertebrate embryos. Development.
928 2018;145: dev156869. doi:10.1242/dev.156869
929 37. Nakada T, Hoshijima K, Esaki M, Nagayoshi S, Kawakami K, Hirose S.
930 Localization of ammonia transporter Rhcg1 in mitochondrion-rich cells of yolk sac,
931 gill, and kidney of zebrafish and its ionic strength-dependent expression. Am J
932 Physiol-Regul, Integr Comp Physiol. 2007;293: R1743–R1753.
933 doi:10.1152/ajpregu.00248.2007
934 38. Fridman S. Ontogeny of the Osmoregulatory Capacity of Teleosts and the Role
935 of Ionocytes. Front Mar Sci. 2020;7: 709. doi:10.3389/fmars.2020.00709
936 39. Laurent P, Chevalier C, Wood CM. Appearance of cuboidal cells in relation to
937 salinity in gills of Fundulus heteroclitus, a species exhibiting branchial Na+ but not
938 Cl− uptake in freshwater. Cell Tissue Res. 2006;325: 481–492. doi:10.1007/s00441-
939 006-0187-3
940 40. Karnaky KJ, Ernst SA, Philpott CW. Teleost chloride cell. I. Response of pupfish
941 Cyprinodon variegatus gill Na,K-ATPase and chloride cell fine structure to various

high salinity environments. J Cell Biol. 1976;70: 144–156. doi:10.1083/jcb.70.1.144

41. Pisam M, Chrétien M, Rambourg A, Clermont Y. Two anatomical pathways for the renewal of surface glycoproteins in chloride cells of fish gills. Anat Rec. 1983;207: 385–397. doi:10.1002/ar.1092070302

42. Hootman SR, Philpott CW. Accessory cells in teleost branchial epithelium. Am J Physiol-Regul, Integr Comp Physiol. 1980;238: R199–R206. doi:10.1152/ajpregu.1980.238.3.r199

43. Pisam M, Rambourg A. Mitochondria-Rich Cells in the Gill Epithelium of Teleost Fishes: An Ultrastructural Approach. Int Rev Cytol. 1991;130: 191–232. doi:10.1016/s0074-7696(08)61504-1

44. Shiraishi K, Kaneko T, Hasegawa S, Hirano T. Development of multicellular complexes of chloride cells in the yolk-sac membrane of tilapia (Oreochromis mossambicus) embryos and larvae in seawater. Cell Tissue Res. 1997;288: 583–590. doi:10.1007/s004410050844

45. Sardet C, Pisam M, Maetz J. The surface epithelium of teleostean fish gills. Cellular and junctional adaptations of the chloride cell in relation to salt adaptation. J cell Biol. 1979;80: 96–117. doi:10.1083/jcb.80.1.96

46. Karnaky KJ. Structure and Function of the Chloride Cell of Fundulus heteroclitus and Other Teleosts. Am Zoöl. 1986;26: 209–224. doi:10.1093/icb/26.1.209

47. Hiroi J, McCormick SD, Ohtani-Kaneko R, Kaneko T. Functional classification of mitochondrion-rich cells in euryhaline Mozambique tilapia (Oreochromis mossambicus) embryos, by means of triple immunofluorescence staining for Na+/K+-ATPase,Na+/K+/2Cl- cotransporter and CFTR anion channel. J Exp Biol. 2005;208: 2023–2036. doi:10.1242/jeb.01611

48. Inokuchi M, Nakamura M, Miyanishi H, Hiroi J, Kaneko T. Functional

967 classification of gill ionocytes and spatiotemporal changes in their distribution after
968 transfer from seawater to freshwater in Japanese seabass. J Exp Biol. 2017;220:
969 4720–4732. doi:10.1242/jeb.167320
970 49. Hwang P. Multicellular complex of chloride cells in the gills of freshwater
971 teleosts. J Morphol. 1988;196: 15–22. doi:10.1002/jmor.1051960103
972 50. Hsu H-H, Lin L-Y, Tseng Y-C, Horng J-L, Hwang P-P. A new model for fish ion
973 regulation: identification of ionocytes in freshwater- and seawater-acclimated
974 medaka (Oryzias latipes). Cell Tissue Res. 2014;357: 225–243. doi:10.1007/s00441-
975 014-1883-z
976 51. Lunsford ET, Bobkov YV, Ray BC, Liao JC, Strother JA. Anion efflux mediates
977 transduction in the hair cells of the zebrafish lateral line. Proc Natl Acad Sci.
978 2023;120: e2315515120. doi:10.1073/pnas.2315515120
979 52. Cox JPL. Hydrodynamic aspects of fish olfaction. J R Soc Interface. 2008;5:
980 575–593. doi:10.1098/rsif.2007.1281
981 53. Reiten I, Uslu FE, Fore S, Pelgrims R, Ringers C, Verdugo CD, et al. Motile-
982 Cilia-Mediated Flow Improves Sensitivity and Temporal Resolution of Olfactory
983 Computations. Curr Biol. 2017;27: 166–174. doi:10.1016/j.cub.2016.11.036
984 54. Dubaissi E, Papalopulu N. Embryonic frog epidermis: a model for the study of
985 cell-cell interactions in the development of mucociliary disease. Dis Model Mech.
986 2011;4: 179–192. doi:10.1242/dmm.006494
987 55. Yasuda M, Inui T, Hirano S, Asano S, Okazaki T, Inui T, et al. Intracellular Cl−
988 Regulation of Ciliary Beating in Ciliated Human Nasal Epithelial Cells: Frequency
989 and Distance of Ciliary Beating Observed by High-Speed Video Microscopy. Int J
990 Mol Sci. 2020;21: 4052. doi:10.3390/ijms21114052
991 56. Inui T, Murakami K, Yasuda M, Hirano S, Ikeuchi Y, Kogiso H, et al. Ciliary

992 beating amplitude controlled by intracellular Cl− and a high rate of CO2 production in
993 ciliated human nasal epithelial cells. Pflügers Arch - Eur J Physiol. 2019;471: 1127–
994 1142. doi:10.1007/s00424-019-02280-5
995 57. Rao R, Bhalla V, Pastor-Soler NM. Intercalated Cells of the Kidney Collecting
996 Duct in Kidney Physiology. Semin Nephrol. 2019;39: 353–367.
997 doi:10.1016/j.semnephrol.2019.04.005
998 58. Montoro DT, Haber AL, Biton M, Vinarsky V, Lin B, Birket SE, et al. A revised
999 airway epithelial hierarchy includes CFTR-expressing ionocytes. Nature. 2018;560:
1000 319–324. doi:10.1038/s41586-018-0393-7
1001 59. Yuan F, Gasser GN, Lemire E, Montoro DT, Jagadeesh K, Zhang Y, et al.
1002 Transgenic ferret models define pulmonary ionocyte diversity and function. Nature.
1003 2023;621: 857–867. doi:10.1038/s41586-023-06549-9
1004 60. Mauduit O, Aure MH, Delcroix V, Basova L, Srivastava A, Umazume T, et al. A
1005 mesenchymal to epithelial switch in Fgf10 expression specifies an evolutionary-
1006 conserved population of ionocytes in salivary glands. Cell Rep. 2022;39: 110663–
1007 110663. doi:10.1016/j.celrep.2022.110663
1008 61. Bautista JL, Cramer NT, Miller CN, Chavez J, Berrios DI, Byrnes LE, et al.
1009 Single-cell transcriptional profiling of human thymic stroma uncovers novel cellular
1010 heterogeneity in the thymic medulla. Nat Commun. 2021;12: 1096.
1011 doi:10.1038/s41467-021-21346-6
1012 62. Lister JA, Robertson CP, Lepage T, Johnson SL, Raible DW. nacre encodes a
1013 zebrafish microphthalmia-related protein that regulates neural-crest-derived pigment
1014 cell fate. Dev Camb Engl. 1999;126: 3757–67.
1015 63. Tsujikawa M, Malicki J. Intraflagellar Transport Genes Are Essential for
1016 Differentiation and Survival of Vertebrate Sensory Neurons. Neuron. 2004;42: 703–

716. doi:10.1016/s0896-6273(04)00268-5

64. Parsons MJ, Pisharath H, Yusuff S, Moore JC, Siekmann AF, Lawson N, et al. Notch-responsive cells initiate the secondary transition in larval zebrafish pancreas. Mech Dev. 2009;126: 898–912. doi:10.1016/j.mod.2009.07.002

65. Lee RTH, Asharani PV, Carney TJ. Basal keratinocytes contribute to all strata of the adult zebrafish epidermis. Hogan B, editor. PloS one. 2014;9: e84858. doi:10.1371/journal.pone.0084858

66. Haas P, Gilmour D. Chemokine Signaling Mediates Self-Organizing Tissue Migration in the Zebrafish Lateral Line. Developmental Cell. 2006;10: 673–680. doi:10.1016/j.devcel.2006.02.019

67. Stuart T, Butler A, Hoffman P, Hafemeister C, Papalexi E, Mauck WM, et al. Comprehensive Integration of Single-Cell Data. Cell. 2019;177: 1888-1902.e21. doi:10.1016/j.cell.2019.05.031

68. Hao Y, Stuart T, Kowalski MH, Choudhary S, Hoffman P, Hartman A, et al. Dictionary learning for integrative, multimodal and scalable single-cell analysis. Nat Biotechnol. 2024;42: 293–304. doi:10.1038/s41587-023-01767-y

69. Hao Y, Hao S, Andersen-Nissen E, Mauck WM, Zheng S, Butler A, et al. Integrated analysis of multimodal single-cell data. Cell. 2021;184: 3573-3587.e29. doi:10.1016/j.cell.2021.04.048

70. Butler A, Hoffman P, Smibert P, Papalexi E, Satija R. Integrating single-cell transcriptomic data across different conditions, technologies, and species. Nat Biotechnol. 2018;36: 411–420. doi:10.1038/nbt.4096

71. Satija R, Farrell JA, Gennert D, Schier AF, Regev A. Spatial reconstruction of single-cell gene expression data. Nat Biotechnol. 2015;33: 495–502. doi:10.1038/nbt.3192

72. Petkova M. Correlative Light and Electron Microscopy in an Intact Larval Zebrafish. Doctoral dissertation, Harvard University, Graduate School of Arts & Sciences. 2020.

73. Kasthuri N, Hayworth KJ, Berger DR, Schalek RL, Conchello JA, Knowles-Barley S, et al. Saturated Reconstruction of a Volume of Neocortex. Cell. 2015;162: 648–661. doi:10.1016/j.cell.2015.06.054

74. Eberle AL, Mikla S, Schalek R, Lichtman J, Tate MLK, Zeidler D. High-resolution, high-throughput imaging with a multibeam scanning electron microscope. J Microsc. 2015;259: 114–120. doi:10.1111/jmi.12224

75. Shapson-Coe A, Januszewski M, Berger DR, Pope A, Wu Y, Blakely T, et al. A petavoxel fragment of human cerebral cortex reconstructed at nanoscale resolution. Science. 2024;384: eadk4858. doi:10.1126/science.adk4858

76. Januszewski, Blakely M and, Lueckmann T and, Jan-Matthis. SOFIMA: Scalable Optical Flow-based Image Montaging and Alignment. 2024. Available: https://doi.org/10.5281/zenodo.10534541

77. Berger DR, Seung HS, Lichtman JW. VAST (Volume Annotation and Segmentation Tool): Efficient Manual and Semi-Automatic Labeling of Large 3D Image Stacks. Front Neural Circuits. 2018;12: 88. doi:10.3389/fncir.2018.00088

78. Schindelin J, Arganda-Carreras I, Frise E, Kaynig V, Longair M, Pietzsch T, et al. Fiji: an open-source platform for biological-image analysis. Nat Methods. 2012;9: 676–682. doi:10.1038/nmeth.2019

79. Schmid B, Schindelin J, Cardona A, Longair M, Heisenberg M. A high-level 3D visualization API for Java and ImageJ. BMC Bioinform. 2010;11: 274. doi:10.1186/1471-2105-11-274

80. Cheung KY, Jesuthasan SJ, Baxendale S, Hateren NJ van, Marzo M, Hill CJ, et

1067 al. Olfactory Rod Cells: A Rare Cell Type in the Larval Zebrafish Olfactory Epithelium
1068 With a Large Actin-Rich Apical Projection. Front Physiol. 2021;12: 626080.
1069 doi:10.3389/fphys.2021.626080